HHS Public Access

Author manuscript

Cell Rep. Author manuscript; available in PMC 2018 October 04.

Published in final edited form as:

Cell Rep. 2018 August 28; 24(9): 2479–2492.e6. doi:10.1016/j.celrep.2018.07.084.

Metabolic and Transcriptional Modules Independently Diversify Plasma Cell Lifespan and Function

Wing Y. Lam[1,6,7], **Arijita Jash**[1], **Cong-Hui Yao**[2], **Lucas D'Souza**[3], **Rachel Wong**[1,3], **Ryan M. Nunley**[4], **Gordon P. Meares**[5], **Gary J. Patti**[2], and **Deepta Bhattacharya**[3,8,*]

[1]Department of Pathology and Immunology, Washington University School of Medicine, St. Louis, MO 63110, USA

[2]Department of Chemistry, Washington University, St. Louis, MO 63110, USA

[3]Department of Immunobiology, University of Arizona College of Medicine, Tucson, AZ 85724, USA

[4]Washington University Orthopedics, Barnes Jewish Hospital, St. Louis, MO 63110, USA

[5]Department of Microbiology, Immunology and Cell Biology, West Virginia University School of Medicine, Morgantown, WV 26505, USA

[6]Present address: Amgen Inc., South San Francisco, CA 94080, USA

[7]Present address: Laboratory of Immunology and Vascular Biology, Department of Pathology, School of Medicine, Stanford University, Stanford, CA, USA

[8]Lead Contact

SUMMARY

Plasma cell survival and the consequent duration of immunity vary widely with infection or vaccination. Using fluorescent glucose analog uptake, we defined multiple developmentally independent mouse plasma cell populations with varying lifespans. Long-lived plasma cells imported more fluorescent glucose analog, expressed higher surface levels of the amino acid transporter CD98, and had more autophagosome mass than did short-lived cells. Low amino acid concentrations triggered reductions in both antibody secretion and mitochondrial respiration, especially by short-lived plasma cells. To explain these observations, we found that glutamine was used for both mitochondrial respiration and anaplerotic reactions, yielding glutamate and aspartate for antibody synthesis. Endoplasmic reticulum (ER) stress responses, which link metabolism to

*Correspondence: deeptab@email.arizona.edu.

AUTHOR CONTRIBUTIONS

W.Y.L., G.P.M., G.J.P., and D.B. designed the study. W.Y.L., A.J., C.H.-Y., L.D., R.M.N., and D.B. performed experiments. W.Y.L., A.J., C.-H.Y., L.D., R.W., G.J.P., and D.B. analyzed the data. W.Y.L. and D.B. wrote the paper, and all other authors edited the paper.

DECLARATION OF INTERESTS

D.B. is a co-founder of Cloak Therapeutics and owns significant equity. A patent application related to the current work has been filed (PCT/US18/23288). G.J.P. is a scientific advisory board member for Cambridge Isotope Laboratories. R.M.N. is a paid consultant for Biocomposites, Cardinal Health; CardioMEMS; DePuy, A Johnson & Johnson Company; Integra Sciences; Medtronic; Smith & Nephew; and Wright Medical Technology, Inc. W.Y.L. is an employee of Amgen Inc.

SUPPLEMENTAL INFORMATION

Supplemental Information includes six figures and can be found with this article online at https://doi.org/10.1016/j.celrep.2018.07.084.

transcriptional outcomes, were similar between long- and short-lived subsets. Accordingly, population and single-cell transcriptional comparisons across mouse and human plasma cell subsets revealed few consistent and conserved differences. Thus, plasma cell antibody secretion and lifespan are primarily defined by non-transcriptional metabolic traits.

In Brief

Plasma cell survival and the consequent duration of immunity vary widely with infection or vaccination. Lam et al. demonstrate that short- and long-lived plasma cells are distinguished by metabolic properties such as nutrient uptake. In contrast, very few conserved transcriptional changes are observed between plasma cells of varying longevity.

Graphical Abstract

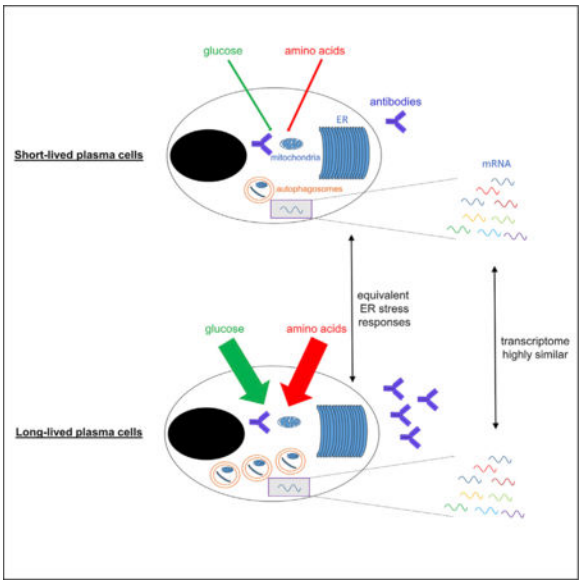

INTRODUCTION

Upon infection or vaccination, naive B cells become activated by foreign antigens, and a subset of these cells differentiate into antibody-secreting plasma cells. Once formed, plasma cells secrete antibodies constitutively as long as they live (Manz et al., 1998; Slifka et al., 1998). Because these antibodies preexist subsequent exposures to pathogens, plasma cells have the ability to provide sterilizing immunity and prevent re-infection. As a result, plasma cells and the antibodies they produce are the primary determinants of humoral immunity following vaccination (Zinkernagel and Hengartner, 2006). The transience of plasma cell persistence and consequent antibody production is the major reason for the loss of immunity against infectious diseases such as malaria (Weiss et al., 2010; White et al., 2015). Reciprocally, long-lived plasma cells pose a major problem in certain autoimmune disorders and are the cell of origin in multiple myeloma (Winter et al., 2012). A mechanistic understanding of plasma cell survival may provide additional targets for the above disorders.

In T cell-dependent reactions, an initial wave of extrafollicular plasma cells tends to be relatively short-lived and produces germline-encoded antibodies (Sze et al., 2000). These cells form an early response to provide partial control of the infection until plasma cells encoding higher affinity antibodies emerge later from the germinal center reaction. As the germinal center progresses, there is a concomitant increase in both the affinity of the encoded antibodies as well as in the lifespans of the selected plasma cells (Weisel et al., 2016). Yet germinal centers are not required per se for the formation of long-lived plasma cells. T cell-independent responses, which yield neither germinal centers nor robust immunological memory, can also yield plasma cells of extended lifespans, as well as a proliferative subset of antibody-secreting cells that together maintain serum antibodies long after immunization (Bortnick et al., 2012; Reynolds et al., 2015; Savage et al., 2017). These and other data demonstrate substantial functional heterogeneity in ontogeny and lifespan within the plasma cell compartment (Amanna et al., 2007), but the underlying molecular basis is unclear.

We reasoned that coupling specific metabolic and transcriptional properties in conjunction with other markers would allow for prospective separation of new plasma cell subsets with a range of lifespans. This in turn would allow for an assessment of how metabolic, transcriptional, and endoplasmic reticulum (ER) stress pathways integrate to regulate plasma cell lifespan and antibody secretion. Using this strategy, we found a very limited correlation between transcriptional changes, ER stress responses, and plasma cell lifespan. Instead, nutrient uptake and catabolism consistently distinguished plasma cell subsets with differing lifespans and antibody secretion rates.

RESULTS

Prospective Separation of Developmentally Distinct Plasma Cell Subsets with Varying Lifespans

We reasoned that prospectively separating plasma cells into functionally distinct groups would provide a cellular foothold to define pathways that regulate lifespan. Intracellular staining for immunoglobulin κ (Igκ) demonstrated very high levels of antibodies in almost all $CD138^{high}$ cells (Figure S1A). We further separated polyclonal $CD138^{+}$ plasma cells in the spleen and bone marrow, formed in response to natural infections in the colony, based on uptake of 2-(*N*-(7-nitrobenz-2-oxa-1,3-diazol4-yl)amino)-2-deoxyglucose (2NBDG), a fluorescent glucose analog (Yoshioka et al., 1996), and expression of B220, which marks relatively short-lived and/or proliferative and immature cells (Chernova et al., 2014; Kallies et al., 2004). Using these criteria, splenic plasma cells could be readily separated into four distinct subsets (Figure S1B). Although all plasma cells imported 2NBDG above background levels, for simplicity we designate the subsets gated as in Figure S1B as either $2NBDG^{+}$ or $2NBDG^{-}$. Bone marrow plasma cells were dominated by the $B220^{-}2NBDG^{+}$ subset, whereas the other subsets were too rare to work with easily (Figure S1B). Therefore, the $B220^{-}2NBDG^{+}$ subset was specifically purified for all subsequent analyses of bone marrow plasma cells.

To quantify the half-lives of plasma cell subsets, we performed pulse-chase experiments using bromodeoxyuridine (BrdU). Mice were provided BrdU in the drinking water for 1

week, followed by either 0, 1, or 2 weeks of water without BrdU (Figure 1A). Animals were then injected with 2NBDG and sacrificed 15 min later. The splenic $B220^{+}2NBDG^{-}$ subset demonstrated the shortest half-life of approximately 3–4 days, followed by the $B220^{-}2NBDG^{-}$ subset (4–6 days), $B220^{+}2NBDG^{+}$ cells (5–18 days), $B220^{-}2NBDG^{+}$ cells (8–12 days), and bone marrow (BM) plasma cells, which showed no turnover during this limited 3-week experiment (Figure 1A). For $B220^{+}2NBDG^{+}$ and $B220^{-}2NBDG^{+}$ cells, the BrdU decay rates varied between weeks 2 and 3. These data suggest additional heterogeneity within these subsets, with a fraction of cells that either proliferate or die rapidly, and another subset that persists more durably without division. Thus, plasma cells that import high levels of 2NBDG have longer half-lives than do their $2NBDG^{-}$ counterparts.

Loss of BrdU retention during the chase period could have been caused by death, proliferation, or differentiation to a distinct plasma cell subset. To distinguish between these possibilities, we first quantified antigen-specific plasma cell numbers over time in each subset after immunization with alum-adjuvanted 4-hydroxy-3-nitrophenylacetyl-ovalbumin (NP-OVA), a T cell-dependent antigen. The initial NP-specific response at 1 week was dominated by the $2NBDG^{-}$ groups, with nearly 80% of antigen-specific plasma cells contained within $B220^{+}2NBDG^{-}$and $B220^{-}2NBDG^{-}$ subsets (Figure 1B). Nevertheless, NP-specific cells could also clearly be found within the $B220^{-}2NBDG^{+}$ and $B220^{+}2NBDG^{+}$ subsets (Figure 1B), suggesting the contemporaneous generation of each of these four plasma cell populations. At these early time points, very few NP-specific bone marrow plasma cells were found (data not shown). Subsequent weeks revealed that NP-specific cells were rapidly lost from the $2NBDG^{-}$ subsets, whereas after an initial decay, antigen-specific cell numbers were relatively stable in both $2NBDG^{+}$ subsets (Figure 1B). These data mirror the BrdU pulse-chase experiments above and suggest that the major portion of plasma cell turnover in each of these subsets is driven by death. Moreover, the contemporaneous formation of multiple plasma cell subsets argues against a strict developmental hierarchy between these groups.

Initial efforts to determine whether plasma cell subsets can interconvert failed because of poor cell recovery after adoptive transfer. Therefore, as an alternative approach, we quantified CD93 expression. CD93 is a marker of developmental maturity and is itself required for long-term maintenance of plasma cells (Chevrier et al., 2009). The percentage of $CD93^{+}$ cells was somewhat lower in 2NBDG plasma cell subsets, but each subset displayed a substantial fraction of mature $CD93^{+}$ cells (Figure 1C). These data again suggest that each plasma cell subset defined by B220 expression and 2NBDG uptake is formed and matures independently of one another.

To further examine the developmental relationships between plasma cell subsets, we performed immunoglobulin repertoire sequencing of polyclonal populations. Within the immunoglobulin G (IgG) isotypes, we observed very little overlap (<10% for most comparisons) between $B220^{+}$ and $B220^{-}$ subsets, both within the spleen and bone marrow (Figures 1D and S1C). These data are consistent with previous studies demonstrating differential light chain usage between $B220^{+}$ and $B220^{-}$ subsets (Chernova et al., 2014). IgM-expressing plasma cells showed somewhat more overlap (15%–25%) between all subsets (Figures 1D and S1C). Although this may reflect somewhat more interconversion

across immunoglobulin M^+ (IgM^+) plasma cell subsets, it seems likely that this overlap occurs because these cells arise from precursor B-1 cells (Savage et al., 2017), which have relatively restricted repertoires (Yang et al., 2015). Within the $B220^+$ or $B220^-$ subsets, we observed 15%–20% overlap between CDR3 nucleotide sequences of $2NBDG^+$ and 2NBDG cells (Figures 1D and S1C). Two of the most diverse subsets were the $B220^+2NBDG^-$ IgG and the $B220^+2NBDG^+$ IgG groups (Figure S1D). Despite their diversity, these two populations showed the most overlap (~25%) of all sets of comparisons (Figure 1D). Reciprocally, the bone marrow IgG group was among the least diverse (Figure S1D), yet showed minimal overlap with any other subset in the same animal (Figure 1D). Thus, it does not appear that diversity per se artificially suppresses the clonal overlap between two groups. These data suggest that developmental interconversion might account for a minor portion of ontogeny, but that the majority of plasma cell immunoglobulin sequences in each subset are unique. We conclude that fluorescent glucose uptake can be used to purify plasma cells of differing lifespans and to help define other pathways that regulate survival, independently of developmental relationships.

Amino Acids Are Limiting for Plasma Cell Respiration and Antibody Secretion

Imported glucose is used both to glycosylate antibodies and to provide spare respiratory capacity, thereby allowing long-lived plasma cells to survive (Lam et al., 2016). This suggests a model in which the very nutrients used to synthesize immunoglobulins are also used to promote survival and energy metabolism in antibody-secreting cells (Lam and Bhattacharya, 2018). To extend upon this model, we assessed plasma cell metabolism of amino acids. We first assessed CD98/SLC3A2 expression, a common subunit for many amino acid transporters (Mastroberardino et al., 1998), and thus a marker of amino acid availability. CD98 expression is controlled by the transcription factor BLIMP1 and thus is very high in plasma cells (Shi et al., 2015; Tellier et al., 2016). CD98 deficiency leads to severe antibody defects, mostly as a function of its adhesion domain being required for activated B cell proliferation (Cantor et al., 2009), but amino acid transport is likely to be essential at the plasma cell stage (Tellier et al., 2016). $2NBDG^-$ plasma cells expressed modestly but consistently lower cell surface levels of CD98 than did $2NBDG^+$ cells (Figure 2A). This difference was not simply a function of cell size, because $B220^+2NBDG^-$, $B220^-2NBDG^+$, and bone marrow plasma cells all showed comparable forward scatter measurements (Figure S2). Amino acids can also be derived intrinsically by autophagy as cellular components are recycled. Although autophagy is normally inversely correlated with extracellular amino acid uptake, $2NBDG^+$ plasma cells modestly but consistently stained more brightly with a dye that marks autophagosomes (An et al., 2017) than did $2NBDG^-$ cells (Figure 2B). These autophagy data are consistent with previous human plasma cell studies (Halliley et al., 2015).

The changes in CD98 expression and autophagy dye staining were subtle and of unclear functional significance. Moreover, many amino acids are transported independently of CD98 and would not be accounted for in these analyses. Therefore, we sought to perform functional assays to test the sensitivity of plasma cell subsets to extracellular amino acid concentrations. Plasma cells that are genetically deficient in autophagy display reduced levels of ATP (Pengo et al., 2013), suggesting that $2NBDG^-$ cells may also display reduced

energy metabolism when amino acids are limiting. Indeed, a retrospective analysis of our previous work revealed that primary plasma cells assayed under physiological amino acid concentrations have lower levels of respiration than cells in standard RPMI media (Figure 2C), which have supraphysiological concentrations of amino acids (Lam et al., 2016). This difference was most pronounced in 2NBDG plasma cells (Figure 2C). To determine whether amino acid availability also limits antibody secretion by plasma cells, we cultured each subset with physiological or supra-physiological concentrations of amino acids in otherwise identical media. A clear association was observed between elevated amino acid concentrations and antibody secretion rates in most subsets (Figure 2D). $2NBDG^+$ plasma cells continued to secrete more antibodies than did $2NBDG^-$ cells under both low- and high-amino acid conditions (Figure 2D). This enhanced secretion by $2NBDG^+$ cells occurred despite apparently elevated levels of autophagy (Figure 2C), which is known to limit immunoglobulin production (Pengo et al., 2013).

Previous studies on myeloma cell lines have demonstrated that glutamine catabolism is essential for energy metabolism, amino acid production, and survival (Garcia-Manteiga et al., 2011; Thompson et al., 2017). ^{13}C-glutamine tracing experiments on primary human long-lived plasma cells demonstrated robust contributions to glutamate and aspartate synthesis, and labeled carbons were readily observed in the tricarboxylic acid (TCA) cycle intermediates malate and fumarate (Figure 3A). However, no label was detected in citrate or aconitate (Figure 3A). Thus, glutamine is used for anaplerotic reactions to generate glutamate and aspartate (Figure 3B). By contributing to succinate oxidation, glutamine also provides electrons for respiration (Lehninger et al., 2013). Although glutamine alone is unlikely to account for the entirety of the link, these data confirm that the same nutrients used to maintain mitochondrial function are also used to generate the amino acid building blocks for immunoglobulin synthesis. It is also likely that amino acid availability promotes antibody secretion through other mechanisms aside from immunoglobulin translation (Zacharogianni et al., 2011).

ER Stress Responses Are Similar across Plasma Cell Subsets

To define how metabolic modules integrate with transcriptional outputs, we first focused on ER stress responses, which can link these pathways. ^{13}C tracing experiments in human bone marrow plasma cells revealed that a substantial portion of uridine diphosphate N-acetylglucosamine (UDP-GlcNac), a precursor to glycosylation sugars, is generated by import of extracellular glucose (Figure S3). Reductions in protein glycosylation and subsequent misfolding of antibodies trigger ER stress responses in plasma cells (Hickman et al., 1977). Given that short-lived plasma cells import relatively little glucose, we reasoned that they may underglycosylate proteins and antibodies, and thus be subject to more ER stress than are their long-lived counterparts. ER stress responses are necessary for high levels of antibody secretion, but they can also limit the lifespan of plasma cells (Auner et al., 2010; Reimold et al., 2001).

Splicing of XBP1 to XBP1s by IRE1α, cleavage of ATF6α into an active transcription factor, and phosphorylation of eIF2α by eukaryotic translation initiation factor 2 alpha kinase 3/protein kinase R-like endoplasmic reticulum kinase (EIF2AK3/PERK) represent

the three arms of the ER stress response (Ron and Walter, 2007). Expression of ATF6α targets, such as HSPA5, varied slightly across subsets, with the lowest levels in $B220^{+}2NBDG^{-}$ and bone marrow plasma cells (Figure 4A), but XBP1s and downstream targets such as EDEM1 were similarly expressed by all groups (Figure 4A). This analysis revealed no significant changes in ER stress responses that correlated with 2NBDG uptake and, as a result, with lifespan (Figure 4A). Previous studies have suggested that caspase-12 activation might promote ER stressdependent apoptosis in short-lived plasma cells (Auner et al., 2010). Yet cleavage of a caspase-12 substrate was similar across all plasma cell subsets (Figure 4B). These data demonstrate that the XBP1s and ATF6α-dependent ER stress pathways are similar between short- and long-lived plasma cells. We next examined the remaining ER stress pathway, mediated by phosphorylation of eIF2α. Although previous studies using *in vitro* cultures found minimal phosphorylation of eIF2α (Ma et al., 2010), we observed clear activation of this pathway in all plasma cell subsets *ex vivo* (Figure 4C). $B220^{+}$ plasma cells displayed slightly elevated levels of p-eIF2α relative to their $B220^{-}$ counterparts (Figure 4C). However, no changes were observed in p-eIF2α as a function of 2NBDG uptake (Figure 4C).

We considered the possibility that short-lived plasma cells succumb to apoptosis because of a relative inability, rather than an excessive propensity, to mount ER stress responses. Neither XBP1 nor ATF6α are required for plasma cell survival (Aragon et al., 2012; Taubenheim et al., 2012), yet the necessity of eIF2α phosphorylation in plasma cells *in vivo* remains unresolved (Gass et al., 2008; Mielke et al., 2011; Scheuner et al., 2001). Therefore, we first defined the relevant kinases involved in eIF2α phosphorylation in plasma cells. We isolated human bone marrow plasma cells, due to their abundance, and examined the effects of pharmacological inhibitors of each of the kinases involved in eIF2α phosphorylation (Ron and Walter, 2007). Inhibition of PERK, but not of general control nonderepressible 2 (GCN2), protein kinase R (PKR), or Heme-regulated inhibitor (HRI), completely eliminated p-eIF2α (Figure 4D). Thus, PERK is solely responsible for eIF2α phosphorylation in plasma cells.

Consistent with previous in vitro-generated plasma cells in lipopolysaccharide (LPS) cultures (Gass et al., 2008), we observed no effect of PERK inhibition on survival or antibody secretion *ex vivo* (Figures S4A and S4B). To test the importance of PERK for plasma cell survival *in vivo*, we utilized conditional $Perk^{fl/fl}$ mice crossed to transgenic animals ubiquitously expressing tamoxifen-inducible CreERT2 (Guthrie et al., 2016). Equal numbers of CD45.2 $Perk^{fl/fl}$ or $Perk^{fl/fl}$ *CAGG-CreERT2* bone marrow cells were mixed with wild-type competitor CD45.1 bone marrow cells and transplanted into irradiated CD45.1 recipients. At 8 weeks post-transplant, mice were given tamoxifen-containing chow for 2 weeks. CD45.2 chimerism was then measured of B lymphocytes and plasma cells formed in response to natural infections in the colony. Chimerism of splenic B cells was similar irrespective of *Perk* genotype (Figure 4E). Within the plasma cell subsets, we observed a small but consistent reduction in PERK-deficient $B220^{+}2NBDG^{-}$ and $B220^{+}2NBDG^{+}$ plasma cells relative to controls (Figures 4E and S4C). In contrast, no statistically significant reductions were observed in PERK-deficient $B220^{-}2NBDG^{-}$ or $B220^{-}2NBDG^{+}$ plasma cells (Figure 4E).Bone marrow plasma cell chimerism was also similar between genotypes, but we were unable to confirm efficient deletion of *Perk* in these

cells (Figure S4D). These data demonstrate that PERK promotes either survival or formation of $B220^+$ plasma cells *in vivo*. However, this dependency on PERK is not correlated with glucose uptake, and thus fails to explain inherent differences in survival between plasma cell subsets.

ER stress in $2NBDG^-$ cells could potentially be mitigated by reducing overall rates of protein and antibody production. Indeed, examination of electron micrographs revealed no consistent alterations in ER lumenal distension (Figures S5A and S5B), a marker of misfolded protein accumulation (Oslowski and Urano, 2011). Each plasma cell subset also displayed similar total levels of Igκ protein and mRNA (Figures 5A and S5C). To test whether the rates of protein translation differ between cell types, we employed *in vivo* ribopuromycylation in which puromycin is incorporated into nascent polypeptides, leading to chain termination (Seedhom et al., 2016). Mice were injected with puromycin and 2NBDG, sacrificed 15 min later, and intracellular levels of puromycin were measured. All plasma cell subsets had similar levels of puromycin labeling, and there was no correlation between 2NBDG uptake and translation rates (Figure 5B). Consistent with these findings, each subset displayed similar levels of phosphorylated S6 (Figure S5D), a marker of mammalian target of rapamycin (mTOR) activation, which promotes translation and antibody synthesis in plasma cells (Jones et al., 2016). Together, these data demonstrate that despite marked differences in glucose uptake, no compensatory changes are engaged in plasma cell subsets to modulate immunoglobulin synthesis and protein translation.

Another mechanism that could mitigate stress responses is protein degradation. To quantify the rates of antibody turnover, we treated plasma cells with the protein translation inhibitor cycloheximide for 24 hr and quantified intracellular levels of Igκ. Although Igκ light chain itself is infrequently glycosylated, it is degraded unless paired with properly folded and glycosylated immunoglobulin heavy chain isotypes (Chillarón and Haas, 2000). As in Figure 5A, antibody levels were similar in all subsets in the untreated control group (Figure 5C). Upon cycloheximide treatment, however, both $2NBDG^-$ subsets showed a substantial loss in Igk relative to their $2NBDG^+$ counterparts (Figure 5C). The loss of antibodies in $2NBDG^-$ plasma cells after cycloheximide could be driven by degradation or by antibody secretion. However, consistent with Figure 2D, $2NBDG^-$ cells secreted substantially fewer antibodies than did their $2NBDG^+$ counterparts (Figure 5D). Thus, $2NBDG^-$ plasma cells degrade antibodies more rapidly than do their $2NBDG^+$ counterparts, and this may be a mechanism by which they avoid excessive ER stress.

Transcriptional Profiles Are Similar between Plasma Cell Subsets

Given that ER stress responses were similar between short- and long-lived plasma cell subsets, we examined the global transcriptional profiles of these subsets in an unbiased way to identify other genes that are correlated with glucose uptake and lifespan. After excluding immunoglobulin genes, RNA-sequencing (RNA-seq) comparisons of short-lived $B220^-2NBDG^-$ and long-lived $B220^-2NBDG^+$ plasma cells revealed remarkably similar transcriptional profiles. A total of 29 genes, representing less than 0.2% of the total transcriptome, showed a statistically significant increase in the $2NBDG^+$ subset (>2-fold change in expression, adjusted p value < 0.05; Figure 6A). Within the $B220^+$ plasma cells,

341 genes were differentially expressed in 2NBDG$^+$ cells relative to their 2NBDG$^-$ counterparts (Figure 6A, middle panel). A comparison of long-lived bone marrow B220$^-$2NBDG$^+$ plasma cells with short-lived splenic B220$^-$2NBDG$^-$ plasma cells revealed more robust changes, with 900 differentially expressed transcripts (Figure 6A, right panel). Pro-apoptotic Bcl-2-like protein 11 (BIM) was modestly decreased in B220$^-$2NBDG$^-$ cells relative to their 2NBDG$^+$ counterparts, but in none of these comparisons did we observe differential expression of a number of other known plasma cell survival factors, such as myeloid leukemia cell differentiation protein 1 (MCL1), B cell maturation antigen (BCMA), CD28, or interleukin-6R (IL-6R) (Minges Wols et al., 2002; O'Connor et al., 2004; Peperzak et al., 2013; Rozanski et al., 2011).

To define a common transcriptional signature used by 2NBDG$^+$ cells, we performed intersection analysis. Only 15 genes were coordinately upregulated and 15 genes downregulated in B220$^-$2NBDG$^+$ or B220$^+$2NBDG$^+$ splenic plasma cells relative to their 2NBDG$^-$ counterparts (Figure 6B). We next compared these 30 genes with transcripts differentially expressed in human long- versus short-lived plasma cells. We observed 66 genes elevated, including pro-survival CD28, and 20 genes downregulated in CD19$^-$ human long-lived plasma cells relative to their CD19$^+$ short-lived counterparts (Figure 6C). Only one gene, *Tmem176b*, demonstrated overlap between genes consistently elevated in mouse 2NBDG$^+$ plasma cells and genes elevated in human long-lived plasma cells (Figure 6D). Thus, we find no evidence for an evolutionarily conserved transcriptional signature associated with enhanced glucose uptake or plasma cell longevity.

Pathway overrepresentation analyses on individual comparisons between plasma cell subsets revealed elevations in cell-cycle gene expression in B220$^+$2NBDG$^-$ cells and, unexpectedly, an elevation in neutrophil degranulation genes in bone marrow plasma cells (Figure 6E). This was surprising given that Ly6gand CD11c-expressing neutrophils and other myeloid cells were specifically excluded from the cells sorted for RNA-seq. Because the levels of transcripts for many of these neutrophil degranulation genes were low, the data suggested that potentially only a subset of plasma cells expressed this unusual signature.

Single-Cell RNA-Sequencing Reveals Plasma Cell Subsets with Distinct Isotypes and Antimicrobial Peptide Expression

We next performed single-cell RNA-seq on approximately 1,000 cells of each plasma cell subset to define transcriptional heterogeneity. Igκ constant region transcripts represented an average of 30% of the total transcriptome of each cell (Figure S6A), consistent with previous plasma cell RNA-seq studies (Shi et al., 2015). Other plasma cell markers including IGJ (Rinkenberger et al., 1996), LY6A/E (Wilmore et al., 2017), TNFRSF13B (Pracht et al., 2017), and XBP1 (Reimold et al., 2001) were highly expressed, confirming the identity and purity of these cells (Figures S6A and S6B).

After excluding immunoglobulin transcripts, t-distributed stochastic neighbor embedding (t-SNE) analysis on concatenated sequences revealed nine clusters (Figure 7A). Three hundred fifty-two genes were preferentially expressed ($p < 0.1$, t test with Benjamini-Hochberg correction for multiple tests) by at least one cluster relative to the rest of the population. Pearson distance measurements using this set of genes revealed that clusters 9 and 6 were

related and distinct from each of the other clusters (Figure 7B). The remaining clusters were distinguished from one another by a much smaller group of genes (Figure 7B). We next overlaid data points from each plasma cell population onto the t-SNE plot to determine the composition of each subset and cluster (Figure 7C). The $B220^{+}2NBDG^{-}$ subset, which is the shortest lived plasma cell population (Figure 1A), was mainly distributed between the unique clusters 6 and 9 (Figures 7C and S6C). In contrast, the long-lived bone marrow plasma cell subset was concentrated in clusters 1 and 5 (Figures 7C and S6C). Each of the other plasma cell populations showed more heterogeneous distributions across the clusters (Figures 7C and S6C). These data demonstrate that despite marked metabolic differences, each plasma cell subset, defined by B220 expression and 2NBDG uptake, is distributed across most of these transcriptionally defined clusters. Thus, plasma cell metabolic properties do not correlate with transcriptional profiles.

To determine how this transcriptional heterogeneity relates to other markers and strategies to separate plasma cell subsets that have been used by others, we examined expression of CD93, major histocompatibility complex class II (MHC class II), CXCR3, and mKi67. CD93 mRNA expression did not uniquely associate with or exclude any clusters (Figure 7D). MHC class II/H2-Aa and CXCR3, which mark $BLIMP1^{low}$ plasmablasts (Kallies et al., 2004; Shi et al., 2015), were preferentially expressed by clusters 6 and 9 (Figure 7D). In contrast, the proliferation marker mKi67 was expressed primarily in cluster 9 (Figure 7D). Other markers, such as CD19 and BLIMP1 itself (Chernova et al., 2014; Kallies et al., 2004; Pracht et al., 2017), were near the lower limit of detection for single-cell RNA-seq, which captures only ~10% of mRNAs (Macosko et al., 2015), and thus did not resolve the populations further (Figure S6B).

We next used all 352 genes that were preferentially and statistically significantly expressed by at least one cluster to perform over-representation analysis, using the Consensus Pathway database (Herwig et al., 2016), to determine the biological significance of the heterogeneity. Biological pathways that were significantly over-represented (q value $< 10^{5}$) included translation, ER protein processing, cell cycle, mRNA splicing, electron transport chain, proteasome, and, as noted above, neutrophil degranulation (Figure 7E). Clusters 6 and 9, which compose most of the short-lived $B220^{+}2NBDG^{-}$ subset (Figure 7D), preferentially expressed genes in the translation, ER protein processing, electron transport chain, and proteasome pathways (Figure 7E). Clusters 6 and 9 were distinguished from each other by genes involved in cell-cycle and mRNA splicing (Figure 7E), consistent with mKi67 expression observed in cluster 9 (Figure 7D). These data suggest that cluster 9 is composed of proliferative $B220^{+}2NBDG^{-}$ plasmablasts, whereas cluster 6 is composed of non-cycling $B220^{+}2NBDG^{-}$ cells. Indeed, reports by others and our own previous data suggest that a subset of the $B220^{+}$ plasma cells is proliferative (Chernova et al., 2014; Lam et al., 2016). As above in Figure 6E, only the neutrophil degranulation pathway was able to distinguish the remaining clusters (Figure 7E). Other highly expressed granulocyte transcripts such as CSF3R and LY6G were undetectable (Figure S6B), arguing against neutrophil contamination.

Inclusion of immunoglobulin constant region genes in the single-cell RNA sequencing (scRNA-seq) analysis revealed differences in isotype usage across plasma cell subsets. For

example, 75% of $B220^{-}2NBDG^{-}$ plasma cells used IgM, whereas nearly 60% of bone marrow plasma cells were IgA^{+} (Figure S6D), consistent with previous reports (Wilmore et al., 2018). However, each isotype was observed at some frequency in every plasma cell subset, demonstrating that antibody class does not strictly define plasma cell longevity or metabolic programs. Expression of neutrophil degranulation genes correlated somewhat with antibody isotype (Figure S6E), but in none of these cases was this correlation absolute. For example, $IgG1^{+}$ plasma cells expressed on average higher levels of *Slpi* than did IgM^{+} plasma cells (Figure S6E). However, a small subset of IgM^{+} cells expressed very high levels of *Slpi* (Figure S6F). Thus, transcriptional programs and antibody isotype independently diversify plasma cell function.

DISCUSSION

Plasma cells vary greatly in lifespan, depending on the type of infection or vaccine, the timing of ontogeny, and their anatomical location. Defining pathways that promote plasma cell longevity is a major goal for vaccine development, especially for immunizations that lead to very transient protection against infections. Reciprocally, identifying ways to antagonize longlived plasma cells in the context of multiple myeloma and autoimmunity is also an important clinical goal. We observed that fluorescent glucose analog uptake correlates with plasma cell lifespan and allows for further purification and prospective isolation of long- and short-lived subsets when coupled with B220 expression. The usage of fluorescent glucose uptake thus helps facilitate the prospective isolation of short- and long-lived plasma cells.

Clearly, however, much still remains unresolved regarding the mechanisms of plasma cell survival. Although glucose uptake correlates with plasma cell longevity, it does not fully explain the heterogeneity. We observed substantial differences in lifespans among plasma cells that import the same amount of glucose. This led us to explore other pathways, such as ER stress and transcriptional regulation of survival genes, which may integrate with metabolism and nutrient uptake to tune plasma cell lifespan. Yet against all our predictions, we found almost no consistent changes in ER stress or transcription between mouse long- and short-lived plasma cell subsets. Although transcriptional changes are essential during plasmablast differentiation to establish a metabolic program (Guo et al., 2018; Jash et al., 2016; Price et al., 2018; Wang and Bhattacharya, 2014), these changes seem not to further distinguish mature plasma cell subsets (Valor et al., 2017).

The transcriptional changes we did observe were mainly linked to cell proliferation and, unexpectedly, genes traditionally involved in neutrophil effector functions. Although we observed no evidence of neutrophil-like granules in plasma cells, it is possible that these proteins are constitutively released and allow certain plasma cell subsets to perform non-canonical effector functions to help clear pathogens and resolve damage. Such properties are reminiscent of tumor necrosis factor alpha (TNF-α)- and inducible nitric oxide synthase (iNOS)-producing IgA^{+} plasma cells in the intestine, which help maintain microbial homeostasis (Fritz et al., 2011). iNOS itself promotes plasma cell survival (Saini et al., 2014), yet it seems unlikely that the innate immune pathways identified here would be directly tied to plasma cell lifespan given that the differences are not correlated with

metabolic properties. The functional importance of these unusual signatures clearly needs to be explored more deeply.

The major pathways that consistently distinguish long- from short-lived plasma cells are non-transcriptional. Long-lived plasma cells that import high levels of glucose and also express high cell surface levels of CD98, a common subunit to many amino acid transporters (Mastroberardino et al., 1998), are less sensitive to reductions in extracellular amino acid concentrations and secrete more antibodies than do their short-lived counterparts. As in human long-lived plasma cells (Halliley et al., 2015), mouse long-lived plasma cells also have elevated autophagosome content. Glucose is used predominantly to glycosylate antibodies, but also to generate pyruvate for spare respiratory capacity, which in turn promotes survival (Lam et al., 2016). Similarly, glutamine is used as a carbon source for mitochondrial anaplerotic reactions and respiration, as well as a building block for antibodies. Together, our findings suggest a metabolic link between antibody secretion and lifespan. The discovery of new pathways that enhance or unlink these properties can potentially be exploited to prolong immunity or antagonize autoimmunity and plasma cell malignancies.

STAR★METHODS

Detailed methods are provided in the online version of this paper and include the following:

- KEY RESOURCES TABLE
- CONTACT FOR REAGENT AND RESOURCE SHARING
- EXPERIMENTAL MODEL AND SUBJECT DETAILS
- METHOD DETAILS
  - Tissue Processing
  - Bone Marrow Chimeras
  - Plasma Cell Cultures
  - Bromodeoxyuridine Experiments
  - Immunizations
  - ELISAs
  - Flow Cytometry/Sorting
  - qRT-PCR
  - Electron Microscopy
  - *In Vivo* Ribopuromycylation
  - CaspGLOW Assay
  - Immunoglobulin Repertoire Analysis
  - RNA-Seq

STAR★METHODS

KEY RESOURCES TABLE

REAGENT or RESOURCE	SOURCE	IDENTIFIER
Antibodies		
CD138 (PE conjugate)	Biolegend	Catalog 352306; RRID:AB_10915989
Donkey Anti-Mouse IgG (H+L)-biotin conjugate	Jackson Immunoresearch	709–065-149; RRID:AB_2340507
streptavidin horseradish peroxidase	BD Biosciences	554066
B220-allophycocyanin (APC)-Cy7	Biolegend	103224; RRID:AB_313007
CD93-PE-Cy7	Biolegend	136506; RRID:AB_2044012
p-S6-V450	BD Biosciences	561457; RRID:AB_10643763
p-eIF2a-Alexa 647	Abcam	ab196191
Igk-PE-Cy7	BD Biosciences	560667; RRID:AB_1727535
CD45.2-BV510	Biolegend	109837; RRID:AB_2561393
CD45.1-BV605	Biolegend	110738; RRID:AB_2562565
Puromycin	Developmental Studies Hybridoma Bank	PMY-2A4; RRID:AB_2619605
biotin mouse anti-mouse IgG2a[b]	BD Biosciences	553504; RRID:AB_394889
BV605 Streptavidin	Biolegend	405229
Chemicals, Peptides, and Recombinant Proteins		
Puromycin	EMD Millipore	540222
Histopaque 1119	Sigma	11191
GSK2606414	Sigma	516535
SP600125	Sigma	S5567
indirubin-3'-monoxime	Sigma	402086
imidazole-oxindole C16	Sigma	I2399
Hemin	Sigma	51280
aluminum potassium sulfate	Fisher	S70459
NP-Ova	Biosearch	N-5051
4-hydroxy-3-nitrophenylacetyl-O-succinimide ester	Biosearch	10634
Allophycocyanin	Sigma	A7472
3,3',5,5'- Tetramethulbenzidine dihydrochloride hydrate	Dako	S1599
paraformaldehyde	Electron Microscopy Services	15710
Saponin	Sigma	84510
13C-U-glucose	Cambridge Isotopes	CLM-1396
13C-U-glutamine	Cambridge Isotopes	CLM-1822
tamoxifen-containing chow	Envigo	TD.130860
Cycloheximide	Fisher	NC0667720
2NBDG	Cayman Chemicals	11046
Critical Commercial Assays		
CD138 enrichment beads	Miltenyi	130–051-301
anti-PE microbeads	Miltenyi	130–048-801
LS columns	Miltenyi	130–042-401
Autophagy Assay kit	Sigma	MAK138
FITC BrdU Flow kit	BD Biosciences	BDB557891
NucleoSpin RNA isolation kit	Macherey-Nagel	740902.50
SYBR Green PCR master mix	Applied Biosystems	4309155

Superscript III Reverse transcription kit	Thermo Fisher	18080400
CaspGLOW 12 staining kit	Biovision	K172–25
SMART-Seq v4	Clontech	634888
Nextera XT DNA library kit	Illumina	131–1024
Chromium Single Cell 3' Library & Gel Bead Kit	10x Genomics	120237
Deposited Data		
RNA-seq data	This paper	NCBI GEO: GSE115860
Single cell RNA seq data	This paper	NCBI GEO: GSE115860
Experimental Models: Organisms/Strains		
Mouse: C57BL/6N	Charles River Labs	Strain code 027
Mouse: B6-Ly5.1/Cr	Charles River Labs	Strain code 564
Mouse: Eif2ak3-tm1.2Drc/J	Jackson Labs	Stock No: 023066
Mouse: B6.Cg-Tg(CAG-cre/Esr1*)5Amc/J	Jackson Labs	Stock No: 004682
Mouse: B6.Cg-Gpi1a Thy1a Igha/J	Jackson Labs	Stock No: 001317
Oligonucleotides		
Primers for XBP1s: 5'-CTGAGTCCGaAtCAGGTGCAG-3' (forward) and 5'-GTCCATGGGAAGATGTTCTGG-3' (reverse)	Sigma	N/A
Primers for XBP1: 5'-TGGCCGGGTCTGCTGAGTCCG (forward) and 5'-GTCCATGGGAAGATGTTCTG-3' (reverse)	Sigma	N/A
Primers for HSPA5: 5'-TTCAGCCAATTATCAGCAAACTCT (forward) and 5'-TTTTCTGATGTATCCTCTTCACCAGT-3' (reverse)	Sigma	N/A
Primers for DDIT3: 5'-CATACACCACCACACCTGAAAG (forward) and 5'-CCGTTTCCTAGTTCTTCCTTGC-3' (reverse)	Sigma	N/A
Primers for EDEM1: 5'-CCTCAATGTGGCCAGAACTT (forward) and 5'-CAGGACCTTTGCACAGGAAT-3' (reverse)	Sigma	N/A
Primers for HPRT: 5'-TTATGGACAGGACTGAAAGAC-3' (forward) and 5'-GCTTTAATGTAATCCAGCAGGT-3' (reverse)	Sigma	N/A
msVHEstdseq1 forward: 5'-TCTTTCCCTACACGATCTGGGAATT CGAGGTGCAGCTGCAGGAGTCTGG-3'	Sigma	N/A
common mu stdseq2 reverse 5'-GTGACTGGAGTTCAGACGTG TGCTCTTCCGATCTAGGGGGAAGACATTTGGGAAGGAC-3'	Sigma	N/A
P5 forward Stdseq: 5'- AATGATACGGCGACCACCGAGATCTA CAC TCTTTCCCTACACGACGC-3'	Sigma	N/A
P7 reverse Stdseq index: CGGCATACGAGATNNNNNNNNGTG ACTGGAGTTCAGACGTGTGTG-3' where N represents a unique index for multiplexing.	Sigma	N/A
Cg1 reverse primer 5'- GGAAGGTGTGCACCGCTGGAC-3'	Tiller et al., 2009	N/A
Cg2c reverse primer 5'-GGAAGGTGCACACTGGAC-3'	Tiller et al., 2009	N/A
Cg2c reverse primer 5'-GGAAGGTGCACACTGGAC-3'	Tiller et al., 2009	N/A
Cg3 primer 5'-AGACTGTGCGCACACCGCTGGAC-3'	Tiller et al., 2009	N/A
common Cgamma reverse primer: 5'- GTGACTGGAGTTCAGA CGTGTGCTCTTCCGATCTCAAGGTGGATAGAGAGCATCGA TGGGG-3'	Sigma	N/A
Stdseq1: 5'-ACACTCTTTCCCTACACGACGCTCTTCCGATCT-3'	Sigma	N/A
Stdseq2: 5'-GTGACTGGAGTTCAGACGTGTGCTCTTCCGATCT-3'	Sigma	N/A
Index seq: 5'-GATCGGAAGAGCACACGTCTGAACTCCAGTCAC-3'	Sigma	N/A
Primers for PERK qRT-PCR: forward 5'- GAAATCTCTGACTACAT ACGGAC-3' reverse 5'- ACACTGAAATTCCACTTCTCAC-3'	Sigma	N/A
Software and Algorithms		
Salmon 0.9.1	https://doi.org/10.1038/ nmeth.4197	https://combine-lab.github.io/salmon/
Deseq2 2.11.40.2	https://doi.org/10.1186/ s13059–014-0550–8	https://usegalaxy.org/?tool_id= toolshed.g2.bx.psu.edu%2Frepos% 2Fiuc%2Fdeseq2%2Fdeseq2% 2F2.11.40.2&version=2.11.40. 2&__identifer=p99wpps8cus
Cell Ranger 2.1.0	10x Genomics	https://support.10xgenomics.com/ single-cell-gene-expression/software/ downloads/latest
Loupe Browser 2.0.0	10x Genomics	https://support.10xgenomics.com/ single-cell-gene-expression/software/ downloads/latest
SeqGeq 1.4.0	FlowJo	https://www.flowjo.com/solutions/ seqgeq/downloads
Prism 7	Graphpad	https://www.graphpad.com/scientificsoftware/prism/
Mixcr 2.1.3	https://doi.org/10.1038/ nmeth.3364	https://mixcr.readthedocs.io/en/latest/ install.html
Clonoplot	https://doi.org/10.1186/ s12859–017-1575–2	https://bitbucket.org/ClonoSuite/ clonocalc-plot
Other		
Custom physiological RPMI media	Thermo Fisher	Lam et al., 2016

CONTACT FOR REAGENT AND RESOURCE SHARING

Further information and requests for resources and reagents should be directed to and will be fulfilled by the Lead Contact, Deepta Bhattacharya (deeptab@email.arizona.edu).

EXPERIMENTAL MODEL AND SUBJECT DETAILS

All animal procedures in this study were approved by the Institutional Animal Care and Use Committee at Washington University (protocol 20160259) and at The University of Arizona (protocol 17–266). 8–12 week old mice of both sexes were used, were age- and sexmatched for each experiment, and littermates were used and chosen randomly in all experiments. C57Bl6/N and B6-Ly5.2/Cr (CD45.1) mice were purchased from Charles River Laboratories, IgH^a allotype mice were purchased from Jackson Laboratories, and then housed in specific pathogen-free facilities for wild-type bone marrow and splenic plasma cells. *Perk*$^{fl/fl}$ mice and CAGG-CreERT2 mice were purchased from Jackson Laboratories. Mice were maintained under specific pathogen-free conditions. Euthanasia was performed by administering carbon dioxide at 1.5L/minute into a 7L chamber until 1 minute after respiration ceased. After this point, cervical dislocation was performed to ensure death.

All human sample procedures in this study were approved by the Human Research Protection Office at Washington University. Bone marrow was obtained from total hip arthroplasty samples from patients undergoing elective surgery (Barnes Jewish Hospital). All samples were kept anonymous with no identifying information. The sex and age of the donors were not determined.

METHOD DETAILS

Tissue Processing—For mouse long-lived plasma cells, femurs, tibiae, humerus, and pelvic bones were isolated and crushed with a mortar and pestle. Spleens were dissected and dissociated using frosted glass microscope slides. Non-cellular debris was removed from bone marrow samples by gradient centrifugation for 10 minutes at 2000 g using Histopaque 1119 (Sigma-Aldrich). Interface cells were collected and red blood cells were lysed using a 0.15 M NH4Cl, 10 mM KHCO3, 0.1 mM EDTA (pH 7.2) solution (ACK). Cells were washed and filtered through 70-μM nylon mesh and stained with 1 μL/10^7 cells anti-CD138-PE (Biolegend). Antibody-bound cells were enriched using 1 μL/10^7 cells anti-PE microbeads and LS columns (Miltenyi Biotec) prior to flow cytometric analysis and sorting. Human bone marrow plasma cells were isolated using CD138 enrichment beads (Miltenyi Biotec) as previously described (Lam et al., 2016).

Bone Marrow Chimeras—For competitive reconstitutions, 5×10^6 bone marrow cells from either *Perk*$^{fl/fl}$ or *Perk*$^{fl/fl}$:CAGG CreER littermates were mixed with 5×10^6 bone marrow cells from B6.Ly5.2 CD45.1^+ mice and injected retro-orbitally into isoflurane-anesthetized 800 cGy-irradiated B6.Ly5.2 CD45.1^+ recipients. At 8 weeks post-transplant, mice were fed tamoxifen-containing chow (400 citrate; Envigo) for 2 weeks before sacrifice and analysis.

Plasma Cell Cultures—Sorted plasma cells were cultured overnight (18–20 hours) in hypoxic conditions (37 C, 5% CO_2, 5% O_2) in 100ul of indicated media. Physiological

amino acid media is a custom preparation supplemented with 1% penicillin/streptomycin solution, 10% FBS, and either 5mM or 25mM glucose as indicated and previously described (Lam et al., 2016). Supraphysiological amino acid media refers to RPMI 1640 (Corning Cellgro 90–022-PB). For p-eIF2α inhibition experiments, cells were cultured for 1 hr in the presence of 4 nM GSK2606414 (for PERK inhibition; Sigma-Aldrich [Axten et al., 2013]); 500 μM SP600125 (for GCN2 inhibition; Calbiochem [Robert et al., 2009]); 500 mM indirubin-3'-monoxime (for GCN2 inhibition; Calbiochem [Robert et al., 2009]); 100 μM imidazole-oxindole C16 (for PKR inhibition; Sigma-Aldrich [Jammi et al., 2003]); and 50 μM hemin (for HRI inhibition; Sigma-Aldrich [Fagard and London, 1981]) before flow cytometric analysis. Cycloheximide was used at 50 μM concentrations. Autophagy Blue was used according to manufacturer's instructions (Sigma-Aldrich).

Bromodeoxyuridine Experiments—Mice were fed with 2 mg/mL BrdU in the drinking water for the durations indicated. Animals were injected with 100 μg 2NBDG intravenously and euthanized 15 min later. Because formaldehyde ablates 2NBDG fluorescence (data not shown), plasma cell subsets were purified by fluorescence activated cell sorting prior to fixation, permeabilization, and intracellular analysis of BrdU incorporation and retention. Splenic plasma cells, memory B cells and CD138-enriched bone marrow plasma cells were first stained for surface expression of respective antibodies. Cells were then purified by Fluorescence-activated cell sorting and then fixed, permeabilized, and stained for incorporated BrdU with the FITC BrdU Flow kit (BD Biosciences) according to the manufacturer's instructions. 2NBDG does not survive fixation, allowing for the use of fluorescein derivative-conjugated antibodies for intracellular analysis after cells were purified by FACS.

Immunizations—Mice were immunized intraperitoneally with 100 μg NP-Ova (Biosearch), adjuvanted with Alhydrogel (Invivogen). NP-APC used for staining was made by conjugating allophycocyanin (Sigma-Aldrich) with 4-hydroxy-3-nitrophenylacetyl-O-succinimide ester (Biosearch Technologies).

ELISAs—Supernatant collected was serially diluted 1:4, 1:16, 1:64 in antibody buffer (PBS + 2% BSA + 0.05% Tween). Standard curves were made with unlabeled mouse IgG (Southern Biotech) to 100, 20, 4, 0.8, 0.16, and 0.032 ng/ml. Ninety-six well high binding plates (Corning) were coated with purified rat α-mouse Ig kappa, light chain (BD Pharmingen) at 5 μg/mL in ELISA coating buffer (0.1M bicarbonate, pH 9.5) overnight at 4 C. Plates were washed four times with PBS + 0.05% Tween before blocking for one hour with PBS + 2% BSA. Blocking buffer was flicked out and samples were plated for one hour at room temperature. Plates were washed four times with PBS + 0.05% Tween. Plates were coated with 0.13 μg/mL Biotin-SP-conjugated AffiniPure Donkey Anti-Mouse IgG (H+L) (Jackson Immunoresearch) in antibody buffer and incubated for one hour at room temperature. This secondary antibody recognizes all isotypes due to light chain reactivity. Plates were then washed four times with PBS + 0.05% Tween. Wells were incubated with 1:1000 streptavidin HRP (BD Pharmingen) in antibody buffer for one hour at room temperature. After incubation, wells were washed 3× with PBS + 0.05% Tween and 3× with PBS followed by development with 100 μL of 3,3',5,5'- Tetramethulbenzidine

dihydrochloride hydrate (TMB) (Dako) and quenched with 2N H_2SO_4. ELISA absorbance values were analyzed at 450 nm. Antibody titers were calculated using standard curves generated with known mouse IgG concentrations.

Flow Cytometry/Sorting—All fluorescence activated cell sorting was performed on a BD FACS Aria II. Cells were sorted into phosphate-buffered saline containing 5% bovine serum. All flow cytometric analysis was performed on a BD FACS Aria II, LSR II, or LSR Fortessa. Data was analyzed using FlowJo software (FlowJo Enterprise). The following α-mouse antigen antibodies were used in this study: CD138phycoerythrin (PE) (281–2; Biolegend); B220-allophycocyanin (APC)-Cy7 (RA3–6B2; Biolegend); CD93-PE-Cy7 (AA4.1; Biolegend); p-S6-V450 (N7–548, BD Biosciences); p-eIF2α-Alexa 647 (E90; Abcam); Igκ-PE-Cy7 (187.1, BD Biosciences); CD45.2-BV510 (104: Biolegend); CD45.1-BV605 (A20; Biolegend). For intracellular stains of p-S6 and p-eIF2α, plasma cell subsets were first purified by FACS, fixed with 2% paraformaldehyde (Electron Microscopy Services), and permeabilized with cold 100% methanol prior to staining. For intracellular stains of Igκ, cells were fixed with 2% paraformaldehyde and permeabilized with 0.1% saponin (Sigma-Aldrich) prior to staining.

qRT-PCR—Total RNA was prepared from double-sorted bone marrow plasma cell (20,000–60,000) and four different splenic plasma cell (10,000– 100,000) populations using NucleoSpin RNA isolation kit (Macherey-Nagel) and first strand cDNA synthesis was performed with Superscript III Reverse transcription kit using oligo (dT) primers or random hexamers (Life Technologies) according to the manufacturer's instructions. qRT-PCR was performed using SYBR Green PCR master mix (Applied Biosystems) on a StepOnePlus Real-Time PCR system (Applied Biosystems). The primer sequences, reported previously (Oslowski and Urano, 2011), are as follows: XBP1s, 5'-CTGAGTCCGAATCAGGTGCAG-3' (forward) and 5'-GTCCATGGGAAGATGTTCTGG-3' (reverse); XBP1, 5'-TGGCCGGGTCTGCTGAGTCCG (forward) and 5'-GTCCATGGGAAGATGTTCTG-3' (reverse); HSPA5, 5'-TTCAGCCAATTATCAGCAAACTCT-3' (forward) and 5'-TTTTCTGATGTATCCTCTTCACCAGT-3' (reverse); DDIT3, 5'-CATACACCACCACACCTGAAAG-3' (forward) and 5'-CCGTTTCCTAGTTCTTCCTTGC3' (reverse); EDEM1, 5'-CCTCAATGTGGCCAGAACTT-3' (forward) and 5'- CAGGACCTTTGCACAGGAAT-3' (reverse); PERK, 5'- GAAATCTCTGACTACATACGGAC-3' (reverse) and 5'-ACACTGAAATTCCACTTCTCAC-3' (forward); HPRT, 5'-TTATGGACAGGACTGAAAGAC-3' (forward) and 5'-GCTTTAATGTAATCCAGCAGGT3' (reverse). Expression of each ER stress gene was normalized to HPRT.

Electron Microscopy—Transmission electron microscopy of mouse splenic plasma cell subsets was performed by the Molecular Microbiology Imaging Facility at Washington University. For ultrastructural analysis, $3–5 \times 10^4$ sorted cells were fixed in 2% paraformaldehyde/2.5% glutaraldehyde (Ted Pella, Redding, CA, USA) in 100 mM cacodylate buffer (pH 7.2) for 1 hr at room temperature. Samples were washed in cacodylate

buffer and postfixed in 1% osmium tetroxide (Polysciences, Warrington, PA, USA) for 1 hr. Samples were then rinsed extensively in dH_20 prior to en bloc staining with 1% aqueous uranyl acetate (Ted Pella) for 1 hr. Following several rinses in dH_20, samples were dehydrated in a graded series of ethanol and embedded in Eponate 12 resin (Ted Pella). Sections of 95 nm were cut with a Leica Ultracut UCT7 ultramicrotome (Leica Microsystems, Bannockburn, IL, USA), stained with uranyl acetate and lead citrate, and viewed on a JEOL 1200 EX transmission electron microscope (JEOL USA, Peabody, MA, USA) equipped with an AMT 8 megapixel digital camera and AMT Image Capture Engine V602 software (Advanced Microscopy Techniques, Woburn, MA, USA). ER lumenal width analysis was performed using ImageJ software, and scored blinded to the cellular subset.

***In Vivo* Ribopuromycylation:** Wild-type IgH^a mice were injected with 1 mg of puromycin (EMD Millipore) intraperitoneally and euthanized 15 min later. Following fixation and permeabilization as previously described (Seedhom et al., 2016), puromycin incorporation was detected using a monoclonal antibody (clone 2A4 from the Developmental Studies Hybridoma Bank at the University of Iowa) followed by a biotin mouse anti-mouse IgG2a[b] (clone: 5.7 from BD Pharmingen) and finally BV605 streptavidin (BD Horizon).

CaspGLOW Assay—Caspase 12 activation was measured using the CaspGLOW staining kit (Biovision). Sorted cells were spun down and cultured in custom physiological media supplemented with 1% Pen/Strep, 5 mM glucose, 500 μM glutamine, and 10% FBS and 1 μL of FITC-ATAD-FMK (from kit) for 1 hr in hypoxic conditions (5% O2, 5% CO2, 37C). Cells were analyzed by flow cytometry and FITC-positive cells indicate active caspase-12.

Immunoglobulin Repertoire Analysis—For these analyses, we sorted all recoverable plasma cells from spleen and bone marrow of femurs, tibiae, humerus, and pelvis bones, generating approximately 30,000 cells of each subset. Sorted cells were lysed and RNA made using the NucleoSpin RNA XS kit (Macherey-Nagel) per manufacturer's instruction. cDNA was generated using Superscript III First-Strand Synthesis System for FT (Thermo Fisher) with oligo dT per manufacturer's instructions. PCR primers as previously reported were modified for MiSeq analysis as described below (Menzel et al., 2014; Tiller et al., 2009). IgM immunoglobulin transcripts were amplified with first round PCR with the following primers: msVHEstdseq1 5'-TCTTTCCCTACACGATCTGGGAATTCGAGGTGCAGCTGCAGGAGTCTGG-3' and common mu stdseq2 5'-GTGACTGGAGTTCAGACGTGTGCTCTTCCGATCTAGGGGGAAGACATTTGGGAAGGAC-3'. PCR products were cleaned using gel/PCR DNA fragments extraction kit (IBI Scientific). PCR products were then used as templates for a second round of amplification with the following primers: P5 forward Stdseq 5'-AATGATACGGCGACCACCGAGATCTACAC TCTTTCCCTACACGACGC-3' and P7 reverse Stdseq index 5'CAAGCAGAAGACGGCATACGAGATNNNNNNNNGTGACTGGAG TTCAGACGTGTGTG-3' where N represents a unique combination for barcoding purposes. For IgG repertoire analysis, cDNA was first amplified using the following primers:

msVHEstdseq1 5’-TCTTTCCCTACACGATCTGGGAATTCGAGGTGCAGCTGCAG GAGTCTGG-3’ and a combination of

Cg1 primer 5’- GGAAGGTGTGCACCGCTGGAC-3’,

Cg2c primer 5’-GGAAGGTGCACACTGGAC-3’,

Cg2b primer 5’- GGAAGGTGCACACTGCTGGAC-3’,

Cg3 primer 5’-AGACTGTGCGCACACCGCTGGAC-3’.

This was followed by a second round of PCR with: msVHEstdseq1 5’-TCTTTCCCTACACGATCTGGGAATTCGAGGTGCAGCTG CAGGAGTCTGG-3’ and a common Cg primer: 5’-GTGACTGGAGTTCAGACGTGTGCTCTTCCGATCTCAAGGTGGATAGAGAG CATCGATGGGG-3’. This was followed by a final amplification cycle with P5 forward Stdseq and P7 reverse Stdseq index. Samples were then pooled, gel purified, and then sequenced using the Illumina Miseq 2 3 250 platform with the following primers: Stdseq1: 5’-ACACTCTTTCCCTACACGACGCTCTTCCGATCT-3’; Stdseq2: 5’-GTGACTGGAGTTCAGACGTGTGCTCTTCCGATCT-3’; and Index seq: 5’-GATCGGAAGAGCACACGTCTGAACTCCAGTCAC-3’. Repertoire information was extracted from fastq files using Mixcr (Bolotin et al., 2015) and displayed using Clonoplot (Fa¨ hnrich et al., 2017). Approximately 150,000 reads were obtained for each sample, which when corrected for isotype usage corresponds to ~7–153 coverage. Given that none of the subsets displayed more than 4,000 distinct CDR3 regions, the data approach sequencing saturation.

RNA-Seq—RNA was prepared from approximately 30,000 plasma cells as described above. Human plasma cell RNA-seq data were obtained from our previous studies (Jash et al., 2016; Lam et al., 2016). Sequencing libraries were generated using a Clontech Smart-Seq kit and Nextera DNA library prep kit (Illumina). Single end 50bp reads were acquired using an Illumina HiSeq 2500. Reads were mapped using Salmon (Patro et al., 2017), and differential gene expression analysis was performed using DESeq2 (Love et al., 2014). Reference transcriptomes and annotation files that include immunoglobulin variable and constant region genes were downloaded from the Gencode Project: (ftp://ftp.sanger.ac.uk/pub/gencode/Gencode_mouse/release_M16/gencode.vM16.pc_transcripts.fa.gz). Intersection analysis was performed using Microsoft Access, and Venn Diagrams were generated using https://www.meta-chart.com/venn#/data. Heatmaps were generated using http://www.heatmapper.ca/.

Single-Cell RNA-Seq—Approximately 5000 LY6G- CD11c- plasma cells of each subset were double-sorted and prepared for RNA-sequencing using a Chromium Single Cell 3’ Library & Gel Bead Kit and a Single Cell Controller from 10x Genomics according to manufacturer’s instructions. Sequencing libraries were prepared using Illumina Nextera kits, and each sample was sequenced in its own Illumina HiSeq 2500 lane. Sequencing files were aggregated, normalized, and processed using the Cell Ranger program (10x Genomics) and visualized using Loupe Browser (10x Genomics). Minimum read cutoffs to focus the analysis on high-quality single cells were left at default settings. Clusters were automatically

defined by a graph-based method. Immunoglobulin isotypes and subset-specific expression of neutrophil degranulation genes were visualized using SeqGeq (FlowJo).

^{13}C Tracing Experiments—Human bone marrow plasma cells were purified using CD138 beads as previously described (Lam et al., 2016). Approximately 2×10^6 cells were cultured in 2ml of physiological media containing either 5mM uniformly labeled ^{13}C glucose or 500 μM uniformly labeled glutamine for 24 hours. Cells were harvested and extracted as previously described (Yao et al., 2016). Samples were separated on a Luna aminopropyl column (3 μm, 150 mm × 1.0 mm I.D., Phenomenex) coupled to an Agilent 1260 capillary HPLC system. The Luna column was used in negative mode with the following buffers and linear gradient: A = 95% water, 5% acetonitrile (ACN), 10 mM ammonium hydroxide, 10 mM ammonium acetate; B = 95% ACN, 5% water; 100% to 0% B from 0–45 min and 0% B from 45–50 min; flow rate 50 μL/min. Mass spectrometry detection was carried out on an Agilent 6540 Q-TOF coupled with ESI source. The identity of each metabolite was confirmed by comparing retention times and tandem MS data with standard compounds. The isotopologue distributions were corrected for natural abundance and isotope impurity.

QUANTIFICATION AND STATISTICAL ANALYSIS

Student's t tests, 1-way ANOVAs with post hoc Tukey's multiple comparison tests, and 2-way ANOVAs with post hoc Sidak's multiple comparison tests were performed using Prism software (Graphpad). Figure legends specify the test used, criteria for statistical significance, and experimental replicates. Figures and/or legends specify the number of technical and biological replicates per experiment. Adjusted p values and fold changes for RNA-seq were calculated using DESeq2 (Love et al., 2014). Significant genes in single cell RNA-seq experiments were identified using Loupe Browser, which applied a Benjamini-Hochberg correction for multiple comparisons to generate adjusted p values.

DATA AND SOFTWARE AVAILABILITY—The accession number for the RNA-seq data reported in this paper is NCBI GEO: GSE115860.

Supplementary Material

Refer to Web version on PubMed Central for supplementary material.

ACKNOWLEDGMENTS

This work was supported by NIH grants R01AI099108 and R01AI129945 (to D.B.), R01ES022181 (to G.J.P.), and R01NS099304 (to G.P.M.). This work was also supported by a Robertson Investigator award from The New York Stem Cell Foundation (to D.B.). R.W. was supported by a predoctoral fellowship from the National Science Foundation (DGE-1143954). We thank the Genome Technology Access Center in the Department of Genetics at Washington University School of Medicine for help with genomic analysis. The Center is partially supported by NCI Cancer Center Support Grant P30 CA91842 to the Siteman Cancer Center and by ICTS/CTSA Grant UL1TR000448 from the National Center for Research Resources (NCRR), a component of the NIH, and NIH Roadmap for Medical Research. This publication is solely the responsibility of the authors and does not necessarily represent the official view of NCRR or NIH.

REFERENCES

Amanna IJ, Carlson NE, and Slifka MK (2007). Duration of humoral immunity to common viral and vaccine antigens. N. Engl. J. Med 357, 1903–1915. [PubMed: 17989383]

An M, Ryu DR, Won Park J, Ha Choi J, Park EM, Eun Lee K, Woo M, and Kim M (2017). ULK1 prevents cardiac dysfunction in obesity through autophagy-meditated regulation of lipid metabolism. Cardiovasc. Res 113, 1137–1147. [PubMed: 28430962]

Aragon IV, Barrington RA, Jackowski S, Mori K, and Brewer JW (2012). The specialized unfolded protein response of B lymphocytes: ATF6a-independent development of antibody-secreting B cells. Mol. Immunol 51, 347–355. [PubMed: 22555069]

Auner HW, Beham-Schmid C, Dillon N, and Sabbattini P (2010). The life span of short-lived plasma cells is partly determined by a block on activation of apoptotic caspases acting in combination with endoplasmic reticulum stress. Blood 116, 3445–3455. [PubMed: 20651073]

Axten JM, Romeril SP, Shu A, Ralph J, Medina JR, Feng Y, Li WH, Grant SW, Heerding DA, Minthorn E, et al. (2013). Discovery of GSK2656157: an optimized PERK inhibitor selected for preclinical development. ACS Med. Chem. Lett 4, 964–968. [PubMed: 24900593]

Bolotin DA, Poslavsky S, Mitrophanov I, Shugay M, Mamedov IZ, Putintseva EV, and Chudakov DM (2015). MiXCR: software for comprehensive adaptive immunity profiling. Nat. Methods 12, 380–381. [PubMed: 25924071]

Bortnick A, Chernova I, Quinn WJ, 3rd, Mugnier M, Cancro MP, and Allman D (2012). Long-lived bone marrow plasma cells are induced early in response to T cell-independent or T cell-dependent antigens. J. Immunol 188, 5389–5396. [PubMed: 22529295]

Cantor J, Browne CD, Ruppert R, Féral CC, Fässler R, Rickert RC, and Ginsberg MH (2009). CD98hc facilitates B cell proliferation and adaptive humoral immunity. Nat. Immunol 10, 412–419. [PubMed: 19270713]

Chernova I, Jones DD, Wilmore JR, Bortnick A, Yucel M, Hershberg U, and Allman D (2014). Lasting antibody responses are mediated by a combination of newly formed and established bone marrow plasma cells drawn from clonally distinct precursors. J. Immunol 193, 4971–4979. [PubMed: 25326027]

Chevrier S, Genton C, Kallies A, Karnowski A, Otten LA, Malissen B, Malissen M, Botto M, Corcoran LM, Nutt SL, and Acha-Orbea H (2009). CD93 is required for maintenance of antibody secretion and persistence of plasma cells in the bone marrow niche. Proc. Natl. Acad. Sci. USA 106, 3895–3900. [PubMed: 19228948]

Chillarón J, and Haas IG (2000). Dissociation from BiP and retrotranslocation of unassembled immunoglobulin light chains are tightly coupled to proteasome activity. Mol. Biol. Cell 11, 217–226. [PubMed: 10637303]

Fagard R, and London IM (1981). Relationship between phosphorylation and activity of heme-regulated eukaryotic initiation factor 2 alpha kinase. Proc. Natl. Acad. Sci. USA 78, 866–870. [PubMed: 6940153]

Fähnrich A, Krebbel M, Decker N, Leucker M, Lange FD, Kalies K, and Möller S (2017). ClonoCalc and ClonoPlot: immune repertoire analysis from raw files to publication figures with graphical user interface. BMC Bioinformatics 18, 164. [PubMed: 28284194]

Fritz JH, Rojas OL, Simard N, McCarthy DD, Hapfelmeier S, Rubino S, Robertson SJ, Larijani M, Gosselin J, Ivanov II, et al. (2011). Acquisition of a multifunctional IgA+ plasma cell phenotype in the gut. Nature 481, 199–203. [PubMed: 22158124]

Garcia-Manteiga JM, Mari S, Godejohann M, Spraul M, Napoli C, Cenci S, Musco G, and Sitia R (2011). Metabolomics of B to plasma cell differentiation. J. Proteome Res 10, 4165–4176. [PubMed: 21744784]

Gass JN, Jiang HY, Wek RC, and Brewer JW (2008). The unfolded protein response of B-lymphocytes: PERK-independent development of antibody-secreting cells. Mol. Immunol 45, 1035–1043. [PubMed: 17822768]

Guo M, Price MJ, Patterson DG, Barwick BG, Haines RR, Kania AK, Bradley JE, Randall TD, Boss JM, and Scharer CD (2018). EZH2 represses the B cell transcriptional program and regulates

antibody-secreting cell metabolism and antibody production. J. Immunol 200, 1039–1052. [PubMed: 29288200]

Guthrie LN, Abiraman K, Plyler ES, Sprenkle NT, Gibson SA, McFarland BC, Rajbhandari R, Rowse AL, Benveniste EN, and Meares GP (2016). Attenuation of PKR-like ER kinase (PERK) signaling selectively controls endoplasmic reticulum stress-induced inflammation without compromising immunological responses. J. Biol. Chem 291, 15830–15840. [PubMed: 27226638]

Halliley JL, Tipton CM, Liesveld J, Rosenberg AF, Darce J, Gregoretti IV, Popova L, Kaminiski D, Fucile CF, Albizua I, et al. (2015). Long-lived plasma cells are contained within the CD19(−)CD38(hi)CD138(+) subset in human bone marrow. Immunity 43, 132–145. [PubMed: 26187412]

Herwig R, Hardt C, Lienhard M, and Kamburov A (2016). Analyzing and interpreting genome data at the network level with ConsensusPathDB. Nat. Protoc 11, 1889–1907. [PubMed: 27606777]

Hickman S, Kulczycki A, Jr., Lynch RG, and Kornfeld S (1977). Studies of the mechanism of tunicamycin in hibition of IgA and IgE secretion by plasma cells. J. Biol. Chem 252, 4402–4408. [PubMed: 325006]

Jammi NV, Whitby LR, and Beal PA (2003). Small molecule inhibitors of the RNA-dependent protein kinase. Biochem. Biophys. Res. Commun 308, 50–57. [PubMed: 12890478]

Jash A, Wang Y, Weisel FJ, Scharer CD, Boss JM, Shlomchik MJ, and Bhattacharya D (2016). ZBTB32 restricts the duration of memory B cell recall responses. J. Immunol 197, 1159–1168. [PubMed: 27357154]

Jones DD, Gaudette BT, Wilmore JR, Chernova I, Bortnick A, Weiss BM, and Allman D (2016). mTOR has distinct functions in generating versus sustaining humoral immunity. J. Clin. Invest 126, 4250–4261. [PubMed: 27760048]

Kallies A, Hasbold J, Tarlinton DM, Dietrich W, Corcoran LM, Hodgkin PD, and Nutt SL (2004). Plasma cell ontogeny defined by quantitative changes in blimp-1 expression. J. Exp. Med 200, 967–977. [PubMed: 15492122]

Lam WY, and Bhattacharya D (2018). Metabolic links between plasma cell survival, secretion, and stress. Trends Immunol 39, 19–27. [PubMed: 28919256]

Lam WY, Becker AM, Kennerly KM, Wong R, Curtis JD, Llufrio EM, McCommis KS, Fahrmann J, Pizzato HA, Nunley RM, et al. (2016). Mitochondrial pyruvate import promotes long-term survival of antibody-secreting plasma cells. Immunity 45, 60–73. [PubMed: 27396958]

Lehninger AL, Nelson DL, and Cox MM (2013). Lehninger Principles of Biochemistry, Sixth Edition (W.H. Freeman).

Love MI, Huber W, and Anders S (2014). Moderated estimation of fold change and dispersion for RNA-seq data with DESeq2. Genome Biol. 15, 550. [PubMed: 25516281]

Ma Y, Shimizu Y, Mann MJ, Jin Y, and Hendershot LM (2010). Plasma cell differentiation initiates a limited ER stress response by specifically suppressing the PERK-dependent branch of the unfolded protein response. Cell Stress Chaperones 15, 281–293. [PubMed: 19898960]

Macosko EZ, Basu A, Satija R, Nemesh J, Shekhar K, Goldman M, Tirosh I, Bialas AR, Kamitaki N, Martersteck EM, et al. (2015). Highly parallel genome-wide expression profiling of individual cells using nanoliter droplets. Cell 161, 1202–1214. [PubMed: 26000488]

Manz RA, Löhning M, Cassese G, Thiel A, and Radbruch A (1998). Survival of long-lived plasma cells is independent of antigen. Int. Immunol 10, 1703–1711. [PubMed: 9846699]

Mastroberardino L, Spindler B, Pfeiffer R, Skelly PJ, Loffing J, Shoemaker CB, and Verrey F (1998). Amino-acid transport by heterodimers of 4F2hc/CD98 and members of a permease family. Nature 395, 288–291. [PubMed: 9751058]

Menzel U, Greiff V, Khan TA, Haessler U, Hellmann I, Friedensohn S, Cook SC, Pogson M, and Reddy ST (2014). Comprehensive evaluation and optimization of amplicon library preparation methods for high-throughput antibody sequencing. PLoS ONE 9, e96727. [PubMed: 24809667]

Mielke N, Schwarzer R, Calkhoven CF, Kaufman RJ, Dörken B, Leutz A, and Jundt F (2011). Eukaryotic initiation factor 2alpha phosphorylation is required for B-cell maturation and function in mice. Haematologica 96, 1261–1268. [PubMed: 21565905]

Minges Wols HA, Underhill GH, Kansas GS, and Witte PL (2002). The role of bone marrow-derived stromal cells in the maintenance of plasma cell longevity. J. Immunol 169, 4213–4221. [PubMed: 12370351]

O'Connor BP, Raman VS, Erickson LD, Cook WJ, Weaver LK, Ahonen C, Lin LL, Mantchev GT, Bram RJ, and Noelle RJ (2004). BCMA is essential for the survival of long-lived bone marrow plasma cells. J. Exp. Med 199, 91–98. [PubMed: 14707116]

Oslowski CM, and Urano F (2011). Measuring ER stress and the unfolded protein response using mammalian tissue culture system. Methods Enzymol. 490, 71–92. [PubMed: 21266244]

Patro R, Duggal G, Love MI, Irizarry RA, and Kingsford C (2017). Salmon provides fast and bias-aware quantification of transcript expression. Nat. Methods 14, 417–419. [PubMed: 28263959]

Pengo N, Scolari M, Oliva L, Milan E, Mainoldi F, Raimondi A, Fagioli C, Merlini A, Mariani E, Pasqualetto E, et al. (2013). Plasma cells require autophagy for sustainable immunoglobulin production. Nat. Immunol 14, 298–305. [PubMed: 23354484]

Peperzak V, Vikström I, Walker J, Glaser SP, LePage M, Coquery CM, Erickson LD, Fairfax K, Mackay F, Strasser A, et al. (2013). Mcl-1 is essential for the survival of plasma cells. Nat. Immunol 14, 290–297. [PubMed: 23377201]

Pracht K, Meinzinger J, Daum P, Schulz SR, Reimer D, Hauke M, Roth E, Mielenz D, Berek C, Côrte-Real J, et al. (2017). A new staining protocol for detection of murine antibody-secreting plasma cell subsets by flow cytometry. Eur. J. Immunol 47, 1389–1392. [PubMed: 28608550]

Price MJ, Patterson DG, Scharer CD, and Boss JM (2018). Progressive upregulation of oxidative metabolism facilitates plasmablast differentiation to a T-independent antigen. Cell Rep. 23, 3152–3159. [PubMed: 29898388]

Reimold AM, Iwakoshi NN, Manis J, Vallabhajosyula P, SzomolanyiTsuda E, Gravallese EM, Friend D, Grusby MJ, Alt F, and Glimcher LH (2001). Plasma cell differentiation requires the transcription factor XBP-1. Nature 412, 300–307. [PubMed: 11460154]

Reynolds AE, Kuraoka M, and Kelsoe G (2015). Natural IgM is produced by CD5- plasma cells that occupy a distinct survival niche in bone marrow. J. Immunol 194, 231–242. [PubMed: 25429072]

Rinkenberger JL, Wallin JJ, Johnson KW, and Koshland ME (1996). An interleukin-2 signal relieves BSAP (Pax5)-mediated repression of the immunoglobulin J chain gene. Immunity 5, 377–386. [PubMed: 8885870]

Robert F, Williams C, Yan Y, Donohue E, Cencic R, Burley SK, and Pelletier J (2009). Blocking UV-induced eIF2alpha phosphorylation with small molecule inhibitors of GCN2. Chem. Biol. Drug Des 74, 57–67. [PubMed: 19519745]

Ron D, and Walter P (2007). Signal integration in the endoplasmic reticulum unfolded protein response. Nat. Rev. Mol. Cell Biol 8, 519–529. [PubMed: 17565364]

Rozanski CH, Arens R, Carlson LM, Nair J, Boise LH, Chanan-Khan AA, Schoenberger SP, and Lee KP (2011). Sustained antibody responses depend on CD28 function in bone marrow-resident plasma cells. J. Exp. Med 208, 1435–1446. [PubMed: 21690252]

Saini AS, Shenoy GN, Rath S, Bal V, and George A (2014). Inducible nitric oxide synthase is a major intermediate in signaling pathways for the survival of plasma cells. Nat. Immunol 15, 275–282. [PubMed: 24441790]

Savage HP, Yenson VM, Sawhney SS, Mousseau BJ, Lund FE, and Baumgarth N (2017). Blimp-1-dependent and -independent natural antibody production by B-1 and B-1-derived plasma cells. J. Exp. Med 214, 2777–2794. [PubMed: 28698287]

Scheuner D, Song B, McEwen E, Liu C, Laybutt R, Gillespie P, Saunders T, Bonner-Weir S, and Kaufman RJ (2001). Translational control is required for the unfolded protein response and in vivo glucose homeostasis. Mol. Cell 7, 1165–1176. [PubMed: 11430820]

Seedhom MO, Hickman HD, Wei J, David A, and Yewdell JW (2016). Protein translation activity: a new measure of host immune cell activation. J. Immunol 197, 1498–1506. [PubMed: 27385780]

Shi W, Liao Y, Willis SN, Taubenheim N, Inouye M, Tarlinton DM, Smyth GK, Hodgkin PD, Nutt SL, and Corcoran LM (2015). Transcriptional profiling of mouse B cell terminal differentiation defines a signature for antibody-secreting plasma cells. Nat. Immunol 16, 663–673. [PubMed: 25894659]

Slifka MK, Antia R, Whitmire JK, and Ahmed R (1998). Humoral immunity due to long-lived plasma cells. Immunity 8, 363–372. [PubMed: 9529153]

Sze DM, Toellner KM, García de Vinuesa C, Taylor DR, and MacLennan IC (2000). Intrinsic constraint on plasmablast growth and extrinsic limits of plasma cell survival. J. Exp. Med 192, 813–821. [PubMed: 10993912]

Taubenheim N, Tarlinton DM, Crawford S, Corcoran LM, Hodgkin PD, and Nutt SL (2012). High rate of antibody secretion is not integral to plasma cell differentiation as revealed by XBP-1 deficiency. J. Immunol 189, 3328–3338. [PubMed: 22925926]

Tellier J, Shi W, Minnich M, Liao Y, Crawford S, Smyth GK, Kallies A, Busslinger M, and Nutt SL (2016). Blimp-1 controls plasma cell function through the regulation of immunoglobulin secretion and the unfolded protein response. Nat. Immunol 17, 323–330. [PubMed: 26779600]

Thompson RM, Dytfeld D, Reyes L, Robinson RM, Smith B, Manevich Y, Jakubowiak A, Komarnicki M, Przybylowicz-Chalecka A, Szczepaniak T, et al. (2017). Glutaminase inhibitor CB-839 synergizes with carfilzomib in resistant multiple myeloma cells. Oncotarget 8, 35863–35876. [PubMed: 28415782]

Tiller T, Busse CE, and Wardemann H (2009). Cloning and expression of murine Ig genes from single B cells. J. Immunol. Methods 350, 183–193. [PubMed: 19716372]

Valor LM, Rodríguez-Bayona B, Ramos-Amaya AB, Brieva JA, and Campos-Caro A (2017). The transcriptional profiling of human in vivo-generated plasma cells identifies selective imbalances in monoclonal gammopathies. PLoS ONE 12, e0183264. [PubMed: 28817638]

Wang Y, and Bhattacharya D (2014). Adjuvant-specific regulation of longterm antibody responses by ZBTB20. J. Exp. Med 211, 841–856. [PubMed: 24711582]

Weisel FJ, Zuccarino-Catania GV, Chikina M, and Shlomchik MJ (2016). A temporal switch in the germinal center determines differential output of memory B and plasma cells. Immunity 44, 116–130. [PubMed: 26795247]

Weiss GE, Traore B, Kayentao K, Ongoiba A, Doumbo S, Doumtabe D, Kone Y, Dia S, Guindo A, Traore A, et al. (2010). The Plasmodium falciparum-specific human memory B cell compartment expands gradually with repeated malaria infections. PLoS Pathog. 6, e1000912. [PubMed: 20502681]

White MT, Verity R, Griffin JT, Asante KP, Owusu-Agyei S, Greenwood B, Drakeley C, Gesase S, Lusingu J, Ansong D, et al. (2015). Immunogenicity of the RTS,S/AS01 malaria vaccine and implications for duration of vaccine efficacy: secondary analysis of data from a phase 3 randomised controlled trial. Lancet Infect. Dis 15, 1450–1458. [PubMed: 26342424]

Wilmore JR, Jones DD, and Allman D (2017). Protocol for improved resolution of plasma cell subpopulations by flow cytometry. Eur. J. Immunol 47, 1386–1388. [PubMed: 28654161]

Wilmore JR, Gaudette BT, Gomez Atria D, Hashemi T, Jones DD, Gardner CA, Cole SD, Misic AM, Beiting DP, and Allman D (2018). Commensal microbes induce serum IgA responses that protect against polymicrobial sepsis. Cell Host Microbe. 23, 302–311.e3. [PubMed: 29478774]

Winter O, Dame C, Jundt F, and Hiepe F (2012). Pathogenic long-lived plasma cells and their survival niches in autoimmunity, malignancy, and allergy. J. Immunol 189, 5105–5111. [PubMed: 23169863]

Yang Y, Wang C, Yang Q, Kantor AB, Chu H, Ghosn EE, Qin G, Mazmanian SK, Han J, and Herzenberg LA (2015). Distinct mechanisms define murine B cell lineage immunoglobulin heavy chain (IgH) repertoires. eLife 4, e09083. [PubMed: 26422511]

Yao CH, Fowle-Grider R, Mahieu NG, Liu GY, Chen YJ, Wang R, Singh M, Potter GS, Gross RW, Schaefer J, et al. (2016). Exogenous fatty acids are the preferred source of membrane lipids in proliferating fibroblasts. Cell Chem. Biol 23, 483–493. [PubMed: 27049668]

Yoshioka K, Saito M, Oh KB, Nemoto Y, Matsuoka H, Natsume M, and Abe H (1996). Intracellular fate of 2-NBDG, a fluorescent probe for glucose uptake activity, in Escherichia coli cells. Biosci. Biotechnol. Biochem 60, 1899–1901. [PubMed: 8987871]

Zacharogianni M, Kondylis V, Tang Y, Farhan H, Xanthakis D, Fuchs F, Boutros M, and Rabouille C (2011). ERK7 is a negative regulator of protein secretion in response to amino-acid starvation by modulating Sec16 membrane association. EMBO J. 30, 3684–3700. [PubMed: 21847093]

Zinkernagel RM, and Hengartner H (2006). Protective ‘immunity’ by preexistent neutralizing antibody titers and preactivated T cells but not by socalled ‘immunological memory’. Immunol. Rev 211, 310–319. [PubMed: 16824138]

Highlights

- Plasma cells with varying lifespans are distinguished by fluorescent glucose uptake
- Lifespan is associated with antibody secretion, autophagy, and nutrient uptake
- Endoplasmic reticulum stress responses are similar across all plasma cell subsets
- Conserved transcriptional changes are not observed in long-lived subsets

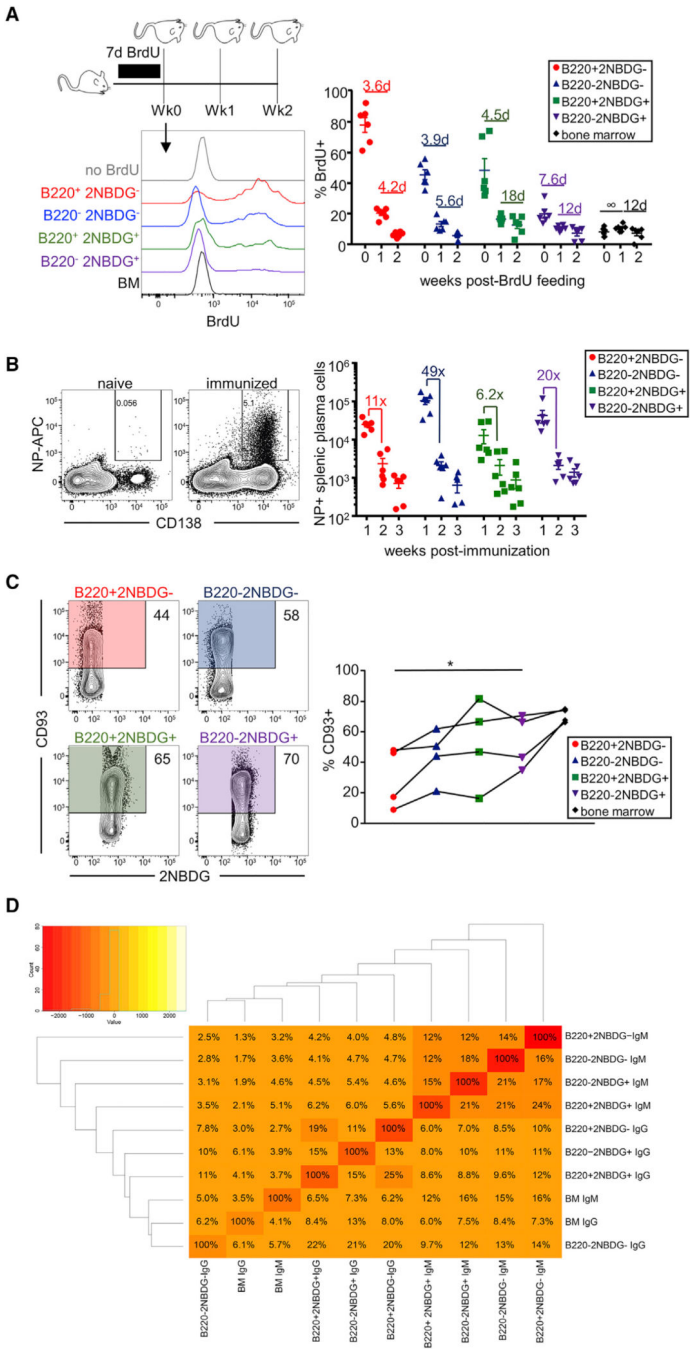

Figure 1. Glucose Uptake Correlates with Long Half-Lives in Plasma Cell Subsets

(A) Mice were fed BrdU in the drinking water for 1 week and assessed for incorporation and retention at 0, 1, and 2 weeks post-BrdU withdrawal. Half-lives of each plasma cell population were calculated at weeks 1 and 2 of the chase period and are shown above each dataset. Data are cumulative from two independent experiments. Mean values ± SEM are shown.

(B) Mice were immunized with NP-OVA, and antigenspecific plasma cells were assessed 1, 2, and 3 weeks thereafter. Example flow cytometric plots (left) and quantification (right) are

shown from CD138-enriched cells and surface NP staining. Data are cumulative from two independent experiments. Mean values ± SEM are shown, as are the fold decreases relative to the previous time point.

(C)Representative CD93 staining of each plasma cellsubset is shown to the left. Cumulative data from two independent experiments are shown to the right. Each data point represents cells from one mouse, and subsets from the same mouse are connected by lines. *$p < 0.05$, by paired one-way ANOVA with post hoc Tukey's multiple comparisons test.

(D)Heatmap showing percent clonal overlap betweenCDR3 nucleotide sequences of plasma cell populations. Plasma cell populations were sorted and immunoglobulin heavy chain VDJ sequences were amplified with common V region primers and either Cm- or pan-Cg-specific primers. Heatmap is derived from one individual mouse out of a total of three analyzed. Data from the remaining mice are shown in Figure S1.

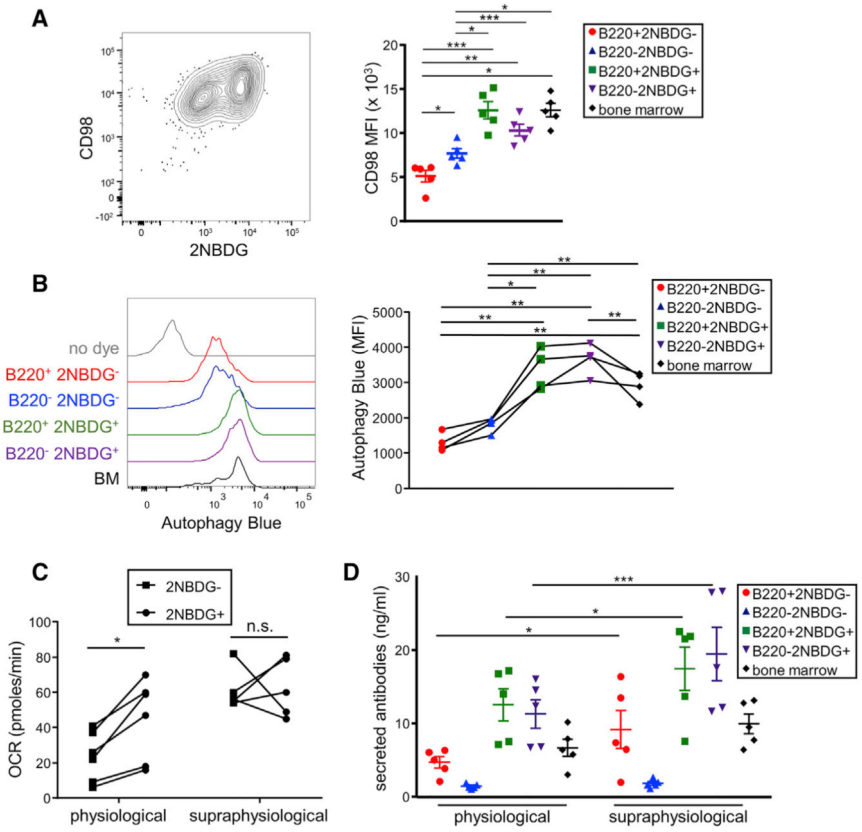

Figure 2. Amino Acids Are Limiting for Plasma Cell Respiration and Antibody Secretion

(A)CD98 expression in plasma cell populations isshown as a representative plot (left) and quantified as mean fluorescence intensity (MFI) values to the right. Data are cumulative from two independent experiments, and each point represents cells from an individual mouse. Mean values ± SEM are shown. *p < 0.05, **p < 0.005, ***p < 0.0005 by oneway ANOVA with post hoc Tukey's multiple comparisons test.

(B)Autophagosome staining of plasma cell populations. Representative graph of autophagy blue staining (left) and quantification of MFI values cumulative from two experiments (right). Each data point represents cells from an individual mouse, and subsets from the same animal are connected by lines. *p < 0.05, **p < 0.005 by paired one-way ANOVA with post hoc Tukey's multiple comparisons test.

(C)Oxygen consumption rates of $2NBDG^+$ or 2NBDG cells cultured either in physiological media or media with supraphysiological concentration of amino acids. Data from the same experiment are connected by lines. *p < 0.05 by Student's two-tailed paired t test.

(D)Antibody secretion analysis of plasma cellpopulations cultured for 24 hr either in physiological media or media with supraphysiological concentrations of amino acids. *p < 0.05, ***p < 0.0005 by two-way ANOVA with post hoc Sidak's multiple comparisons test.

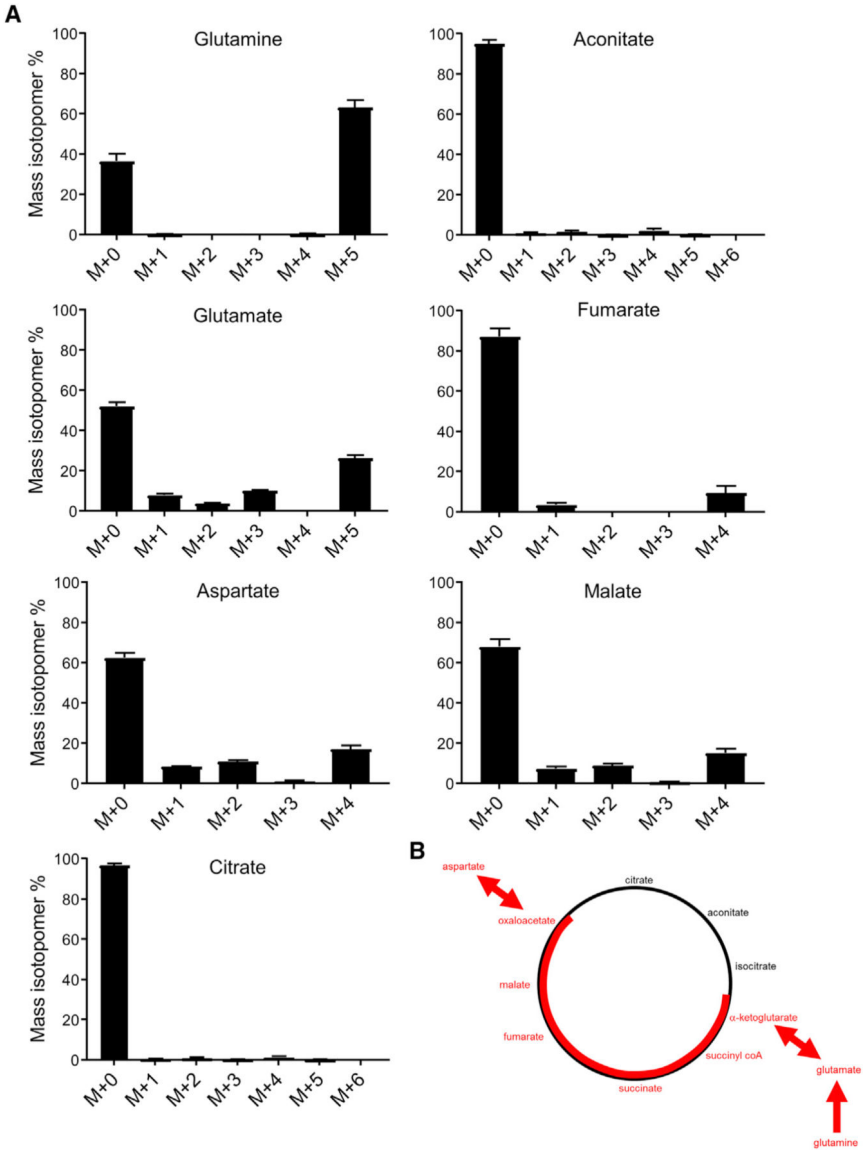

Figure 3. Glutamine Catabolism Links Mitochondrial Function to Amino Acid Biosynthesis

(A) Liquid chromatography-mass spectrometry analysis of ^{13}C enrichment in human bone marrow plasma cell intermediary metabolites. Plasma cells were cultured for 18 hr with uniformly labeled ^{13}C-glutamine-containing media. Isotopologue distributions were corrected for natural abundance and isotope impurity. Mean values of four biological replicates ± SEM are shown.

(B) Schematic of glutamine contribution to the TCA cycle in plasma cells. Red indicates intermediates in which glutamine-derived carbons are found.

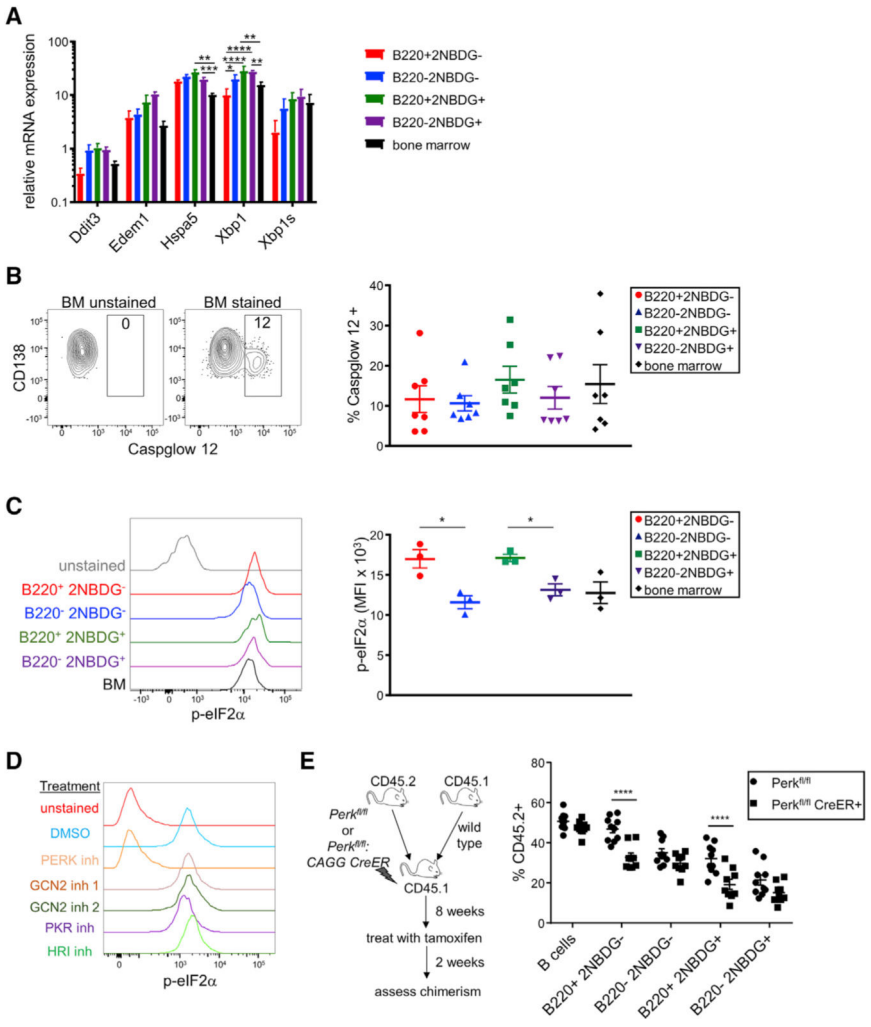

Figure 4. ER Stress Responses Are Similar across Plasma Cell Subsets

(A)qRT-PCR analysis of ER stress response genesin plasma cell subsets. Data are cumulative from two individual experiments, each with three biological replicates of each plasma cell subset. Data are normalized to expression of HPRT. *p < 0.05, **p < 0.005, ***p < 0.0005, ****p < 0.00005 by twoway ANOVA with post hoc Sidak's multiple comparisons test.

(B)Caspase-12 activation in plasma cell populations. Plasma cell populations were sorted and labeled for 1 hr with the fluorescent caspase-12 inhibitor ATAD-FMK. Representative plots (left) and quantification (right) are shown, with each data point representing cells from an individual mouse. Mean values ± SEM are shown. No significant differences were observed using one-way ANOVA.

(C)Flow cytometric representative plots (left) andquantification (right) of p-eIF2α mean fluorescence intensities (MFIs) in plasma cell subsets. *p < 0.05 by one-way ANOVA with post hoc Tukey's multiple comparisons test.

(D) Human bone marrow plasma cells were treatedwith inhibitors to PERK (4 nM GSK2606414), GCN2 (500 μM SP600125 or indirubin-3'-monoxime), HRI (50 μM hemin),

or PKR (100 μM imidazole-oxindole C16) for 1 hr and analyzed for intracellular p-eIF2α. Plots of p-eIF2α representative of two independent experiments are shown.
(E) Schematic representation of mixed bone marrow chimera experiment to assess plasma cell population dependence on PERK (left). $CD45.2^+$ chimerism values are shown (right) and are cumulative from two experiments. Each symbol represents a distinct mouse. ****$p < 0.00005$ by two-way ANOVA with post hoc Sidak's multiple comparisons test.

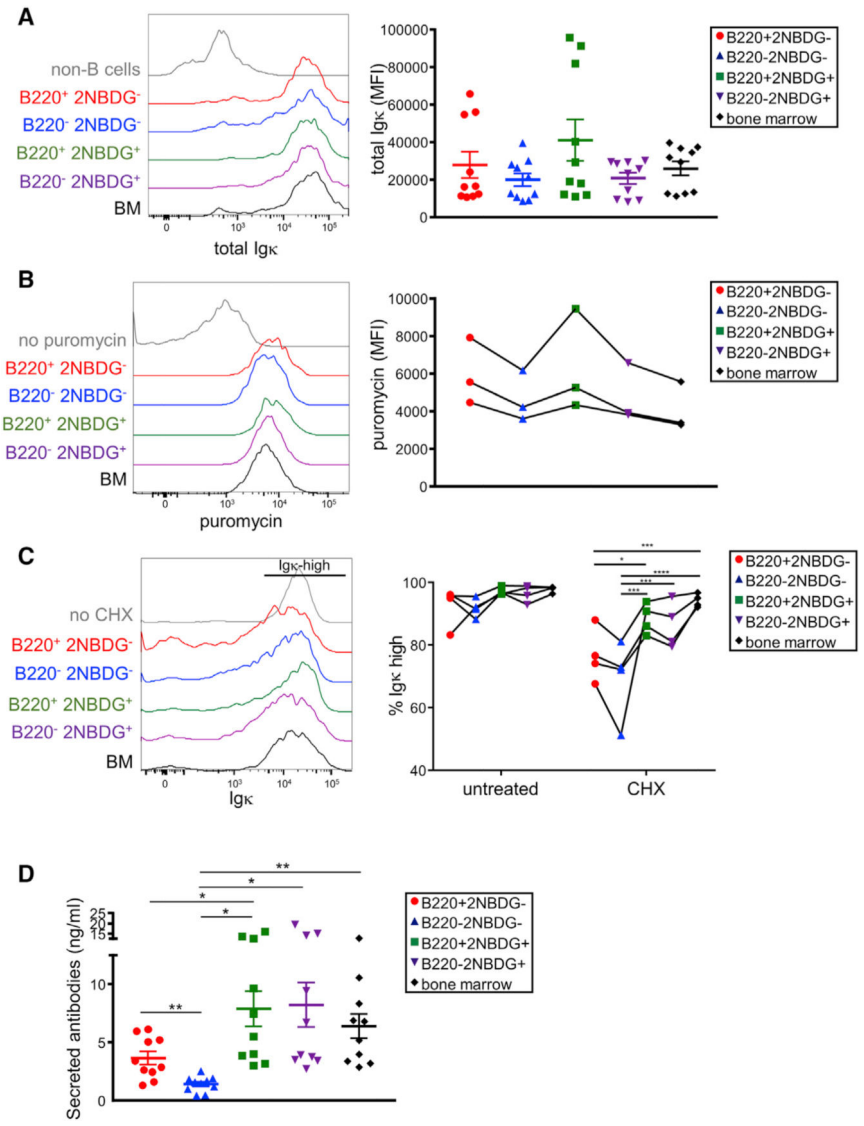

Figure 5. Plasma Cells with Diminished Glucose Uptake Maintain Translation Rates but Secrete Relatively Few Antibodies

(A) Representative plots (left) and quantification of mean fluorescence intensity (MFI) values (right) of total surface and intracellular Igk staining of splenic and bone marrow CD138^{+} plasma cells. Each point represents an individual mouse, and data are cumulative of three independent experiments. Mean values ± SEM are overlaid. No significant differences were observed by one-way ANOVA.

(B) Mice were injected with puromycin and 2NBDG, and sacrificed 15 min later. Representative puromycin staining (left) and quantification of MFI values (right) of splenic and bone marrow plasma cells are shown. Data are from one representative experiment of three total. Each point represents an individual mouse, and subsets from the same mouse are linked by lines. No significant differences were observed by paired one-way ANOVA.

(C) Plasma cell populations were sorted and cultured for 24 hr with or without protein translation inhibitor cycloheximide. Representative total surface and intracellular Igk staining (left) and quantification (right) of splenic and bone marrow plasma cells. Each point

represents an individual mouse, and data are cumulative of two independent experiments. Subsets from the same mouse are linked by lines. *p < 0.05, ***p < 0.0005, ****p < 0.00005 by paired two-way ANOVA with post hoc Sidak's multiple comparisons test. (D) Antibody secretion measured by ELISA after overnight culture of plasma cell subsets from spleen and bone marrow. Each point represents a plasma cell subset from one individual mouse. *p < 0.05, **p < 0.005 by one-way ANOVA with post hoc Tukey's multiple comparisons test. Data are cumulative from three independent experiments.

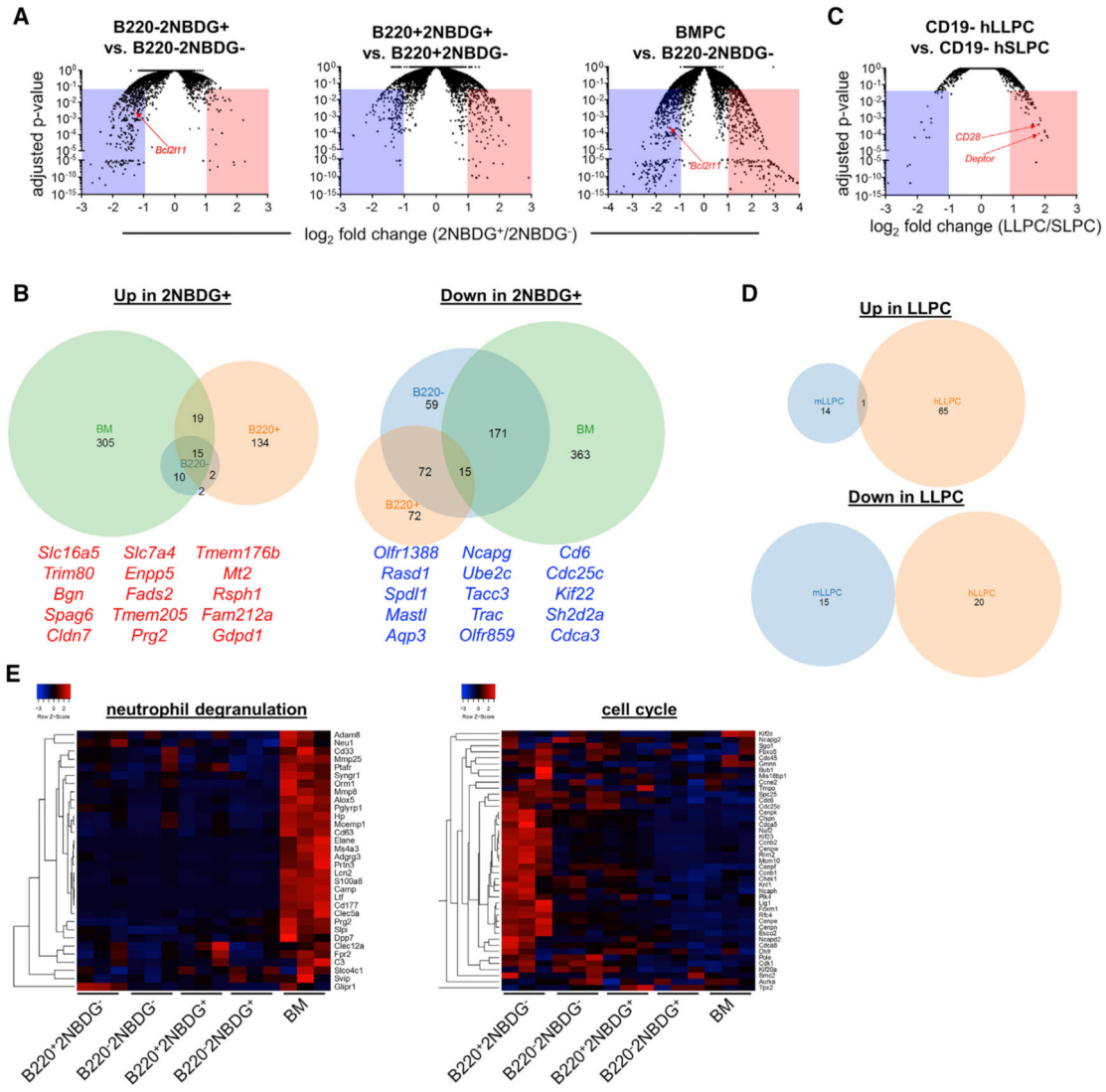

Figure 6. Transcriptional Profiles Are Similar between Plasma Cell Subsets

(A)RNA-seq analysis of gene transcript levels between $B220^{-}2NBDG^{-}$ versus $B220^{-}2NBDG^{+}$, $B220^{+}2NBDG^{-}$ versus $B220^{+}2NBDG^{+}$, or $B220^{-}2NBDG^{-}$ versus BM. Volcano plots of gene expression fold changes between $2NBDG^{+}$ and $2NBDG^{-}$ populations are shown. Adjusted p values were calculated using DESeq2, with red and blue boxes representing genes that are significantly upregulated or downregulated, respectively, in $2NBDG^{+}$ cells. Each dot represents a single gene. Three biological replicates were analyzed for each population.

(B)Venn diagram analysis of common transcripts either upregulated (left) or downregulated (right) in $2NBDG^{+}$ populations.

(C)RNA-seq analysis of gene transcript levels between human $CD19^{+}$ short-lived plasma cells (SLPCs) and $CD19^{-}$ long-lived plasma cells (LLPCs). Volcano plot analysis of differential transcript expression between human LLPCs and SLPCs is shown. Each dot represents a single gene. Four biological replicates were analyzed for each population.

Adjusted p values were calculated using DESeq2. Each dot represents a single gene. Four biological replicates were analyzed for each population.

(D)Little overlap between overexpressed genes in 2NBDG^{+} murine and human long-lived plasma cell populations (top) or 2NBDG^{-} murine and human short-lived plasma cell populations (bottom).

(E)Pathway analysis of genes downregulated in bone marrow plasma cells. Heatmap representation of genes and their expression across each biologicalreplicate of each plasma cell population. Color scale legend depicts row-normalized Z scores.

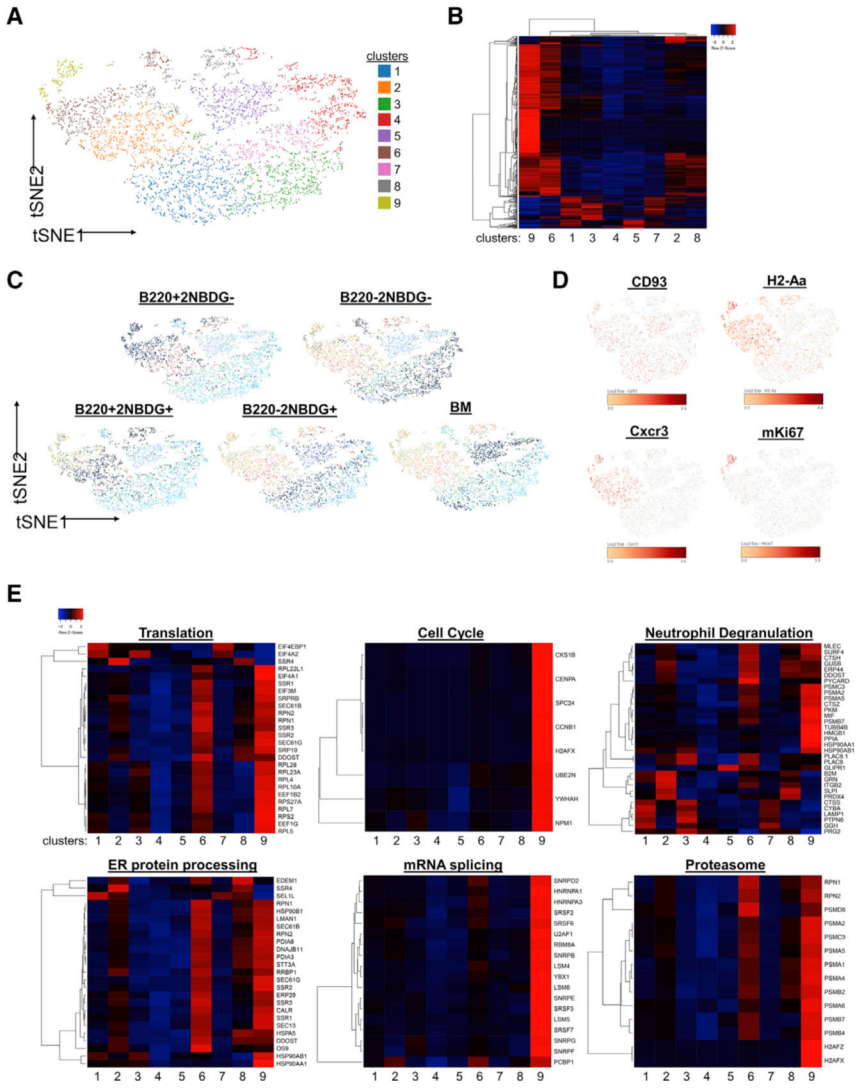

Figure 7. Plasma Cell Transcriptional Heterogeneity Is Defined by Proliferative Genes and Neutrophil Degranulation Pathways

(A) t-SNE analysis of single-cell RNA-seq data concatenated from all plasma cell subsets. Each data point represents one cell, and nine identified clusters are depicted in distinct colors.

(B) All 352 genes were plotted that were statistically significantly and preferentially expressed by at least one cluster relative to the remaining population (adjusted $p < 0.1$, Benjamini-Hochberg test). Each gene and cluster were ordered and grouped based on average linkage and depicted in the corresponding dendrograms. Red indicates high relative expression, and blue indicates low expression, shown as row-normalized Z scores.

(C) Data points from each plasma cell subset were overlaid as dark blue dots onto the concatenated t-SNE plot.

(D) Expression of plasma cell marker genes aredepicted as a heatmap overlaid onto the concatenated t-SNE plot.

(E) Pathway analysis of 352 significant clusterspecific genes. These genes were over-represented in translation, cell cycle, electron transport chain, ER protein processing, mRNA

splicing, proteasome, and neutrophil degranulation pathways as analyzed using the Consensus Pathway database (q value < 10^5). Red indicates high relative expression, and blue indicates low expression, shown as row-normalized *Z* scores.